INDEPENDENT COMPONENT ANALYSIS, THE VALIDATION ON VOLUME CONDUCTOR PLATFORM AND THE APPLICATION IN AUTOMATIC ARTIFACTS REMOVAL AND SOURCE LOCATING OF EEG SIGNALS

CAO CHENG

(B.Eng. USTC)

A THESIS SUBMITTED

FOR THE DEGREE OF MASTER OF ENGINEERING

DEPARTMENT OF MECHANICAL ENGINEERING

&DIVISION OF BIOENGINEERING

NATIONAL UNIVERSITY OF SINGAPORE

2005

ACKNOWLEDGMENTS

First of all, I would like to express my sincere gratitude to my supervisor, Associate Professor Li Xiaoping from the Department of Mechanical Engineering, NUS, who has broad knowledge in many fields and has given me invaluable advices and inspiration in guiding me all the time during the course of this research. His patience, encouragement and support always give me great motivation and confidence in conquering the difficulties encountered in the research. His kindness will always be remembered.

I would also like to thank Associate Professor Einar Wilder-Smith from the Department of Medicine, NUS and Associate Professor Ong Chong Jin from the Department of Mechanical Engineering, NUS for their advices and kind helps to this research.

I am also grateful to my colleagues, Mr. Shen Kaiquan, Mr. Zheng Hui, Mr. Mervyn Yeo Vee Min, Mr. Ng Wu Chun, Miss Xin Bo, Miss Pang Yuanyuan and Miss Zhou Wei, for their kind help.

TABLE OF CONTENTS

1 INTRODUCTION

1.1 The difficulties in EEG signal processing and the previous resolutions 1

1.2 Research objective 4

2 LITERATURE REVIEW

2.1 Previous work on ECG artifact removal 5

2.2 Previous work on Ocular artifacts 6

2.3 The EEG source reconstruction 12

2.4 The validation of EEG signal processing methods 14

2.5 Mathematical background of independent component analysis 15

3 VOLUME CONDUCTOR PLATFORM FOR VALIDATION OF EEG SIGNAL PROCESSING ALGORITHMS

3.1 The volume conductor simulation platform 18

3.2 Experiment setup 20

3.3 The results and discussions 21

4 ICA BASED AUTOMATIC ARTIFACT REMOVAL

4.1 Model of ECG artifact 27

4.2 Automatic ECG artifact removal algorithm 28

4.3 Models of ocular artifacts 31

4.4 Automatic Ocular artifacts removal algorithm 40

5 ICA BASED LORETA FOR SPECIFIC LOCATING BRAIN ACTIVITY SOURCE

5.1 The ICA-LORETA method 46

5.2 Verification by numerical simulation results 48

5.3 Experimental verification using a volume conductor 53

5.4 Extraction of brain activities in response to irregular auditory stimulus 57

6 CONCLUSIONS 66

7 FUTUREWORK 70

REFERENCES 71

LIST OF PUBLISHED WORK IN THE THESIS 78

SUMMARY

Independent Component Analysis (ICA) is a new and powerful blind signal separation algorithm. It decomposes multi- channel mixed signals into independent components which are corresponding to original sources of the mixed signals without any pre-knowledge about the sources and the way of mixture. ICA has been introduced into (electroencephalo-graph) EEG signal processing recently, but the application is only in off-line artifacts removal.

In this research, ICA was verified by experiments on a novel volume conductor platform which has similar electrical characteristic and multi-layer structure to the human brain. It was shown that ICA can decompose signals mixed on the human brain with satisfying accuracy. ICA was used to automatically remove ECG and ocular artifacts online in this research. The independent components corresponding to ECG and ocular artifacts were automatically identified by specific models and then removed.

An ICA based Low Resolution Electromagnetic Tomography Method (LORETA) was also developed in this research for locating the event stimulated brain activities and spontaneous brain activities from single-trial EEG signal. The EEG signal was first decomposed by ICA and the independent components corresponding to brain activities were manually identified by pre-knowledge. The coefficient maps of these independent components were used as input of the LORETA, and the source distribution in the brain was obtained. The detailed algorithm was described and verified by numerical simulation and experiments using a volume conductor platform as well as functional Magnetic Resonance Image (fMRI) with satisfying accuracy.

NOMENCLATURE

SYMBOLS

$\mathbf{X}^T$	Transpose of matrix **X**
$\|\mathbf{w}\|$	Module of vector **w**
E	Mathematic Expectation
ε	Noise
σ^2	Standard variance
R^2	Multiple correlation coefficient
$\boldsymbol{A}^+$	Moore–Penrose pseudoinverse of matrix $\boldsymbol{A}$

ABBREVIATIONS

std	Standard Deviation
ICA	Independent Component Analysis
EEG	Electroencephaloraph
ME	Magnetoencephalograph
ECG	Electrocardiograph
EOG	Electro-Oculogram
OA	Ocular Artifacts
LORETA	Low Resolution Brain Electromagnetic Tomography
fMRI	functional Magnetic Response Image

LIST OF FIGURES

Figure 1.1 EEG signal and artifacts 2

Figure 2.1 Adaptive filter eye artifact canceller 9

Figure 3.1 Models of human brain and watermelon 19

Figure 3.2 Experimental setup for the validation of the volume conductor brain activity simulation platform 20

Figure 3.3 The location of the sources 23

Figure 3.4 Result of ICA Experiment 25

Figure 3.5 (a) Power spatial maps at three frequency bands. The maps are gray scaled, dark represents large amplitude. (b)The real source location on the watermelon 26

Figure 4.1 ICA components and coefficient maps 28

Figure 4.2 The ECG artifact removal 30

Figure 4.3 Original signal, the length is 1024 points 34

Figure 4.4 The performance of wavelet de-noising under different noise energy level 35

Figure 4.5 Wavelet De-noising for eye blinking 38

Figure 4.6 Wavelet De-noising for eye rolling 39

Figure 4.7 The electrode placement scheme used 40

Figure 4.8 The result for a single epoch of contaminated EEG 43

Figure 5.1 Single Sphere model with two current dipoles D1 and D2 48

Figure 5.2 The waveforms of S1 and S2 48

Figure 5.3 Four channels of the simulated EEG signals, the vertical line

indicates the specific time instant at t=300ms 49

Figure 5.4 The tomography reconstructed by LORETA 49

Figure 5.5 The two independent components separated by ICA. The first one is source S1 and the second one was source S2 50

Figure 5.6 The coefficients map of the independent components (a) the first independent component (b) the second independent component 50

Figure 5.7 The tomography reconstructed by LORETA using the coefficient maps (a) the first independent component (b) the second Independent component 52

Figure 5.8 Devices of watermelon experiment 53

Figure 5.9 Six channels of measured mixed signals on the surface of watermelon, the sampling rate was 100Hz 54

Figure 5.10 The first four independent components; the sampling rate is 100Hz 54

Figure 5.11 The coefficient maps of the independent components corresponding to sources. (a) C2 (b) C4 55

Figure 5.12 Raw EEG montage data (experiment pop1).Two vertexes were observed in Fz-Cz and Cz-Pz channels due to the pop sound stimulus at 6th second. 57

Figure 5.13 Component C6 is the brain response due to the pop sound stimulus according to Fig 5.12. C3 was the heartbeat artifacts (ECG). 57

Figure 5.14 Raw EEG montage data (experiment pop2). Two vertexes were observed in Fz-Cz and Cz-Pz channels due to the pop sound stimulus at about 7th second. 58

Figure 5.15 Component C1 was the brain response due to the pop sound stimulus according to Fig 5.14. C0 was the heartbeat artifacts (ECG) 58

Figure 5.16 Raw EEG montage data (experiment clap1). Two vertexes were observed in Fz-Cz and Cz-Pz channels due to the clap sound stimulus after 8h second. 59

Figure 5.17 Component C2 was the brain response due to the clap sound stimulus according to Fig 5.16. C1 was the heartbeat artifacts (ECG) 59

Figure 5.18 Raw EEG montage data (experiment clap2). Two vertexes were observed in Fz-Cz and Cz-Pz channels due to the clap sound stimulus 60

Figure 5.19 Component C5 was the brain response due to the clap sound stimulus according to Fig 5.18. C1 was the heartbeat artifacts (ECG) 60

Figure 5.20 Coefficient maps of ICA components corresponding to response 60

Figure 5.21 Tomography of ICA component C6 in experiment (Pop1) reconstructed by LORETA 62

Figure 5.21 Tomography of ICA component C1 in experiment (Pop2) reconstructed by LORETA 62

Figure 5.23 Tomography of ICA component C2 reconstructed by LORETA, in experiment (Clap1) 63

Figure 5.24 Tomography of ICA component C5 reconstructed by LORETA, in experiment (Clap2) 64

Figure 5.25 fMRI pictures showing activation regions corresponding to infrequent target stimulus, where the bright regions were in activation and dark regions were in deactivation. 64

LIST OF TABLES

Table 4.1 Normalized variance of the ICA components 31

Table 4.2 $R^2$of the ICA component 43

Chapter 1

INTRODUCTION

1.1 The difficulties in EEG signal processing

The electroencephalogram (EEG) was first measured in humans by Hans Berger in 1929. Electrical impulses generated by nerve firings in the brain diffuse through the head and can be measured by electrodes placed on the scalp. The EEG gives a coarse view of neural activity and has been used to non-invasively study cognitive processes and the physiology of the brain. However, the analysis of EEG data and the extraction of useful information from this data is a difficult problem. There are three challenging problems in the analysis of EEG data: first, the EEG artifacts removal, second the EEG source reconstructions, third the validation of EEG signal processing methods.

In any actual measurement of signals, the contamination of artifacts and noises is an avoidless problem especially for the faint signals. Moreover this problem in the measurement of EEG signal is exacerbated by the introduction of extraneous biologically generated and externally generated signals into the EEG. These sources of noises and artifacts include eye blinks, eye movements, heart beat, breathing, and other muscle activities. Some artifacts, such as eye blinks, produce voltage changes of much higher amplitude than the endogenous brain activity. In this situation, the data must be discarded unless the artifacts can be removed from the data. There are various kinds of algorithms to remove artifacts from EEG. Among them, Independent Component Analysis (ICA) is the most popular one. But ICA requires manually selection of independent components corresponding to artifacts and can not be used in online artifacts removal.

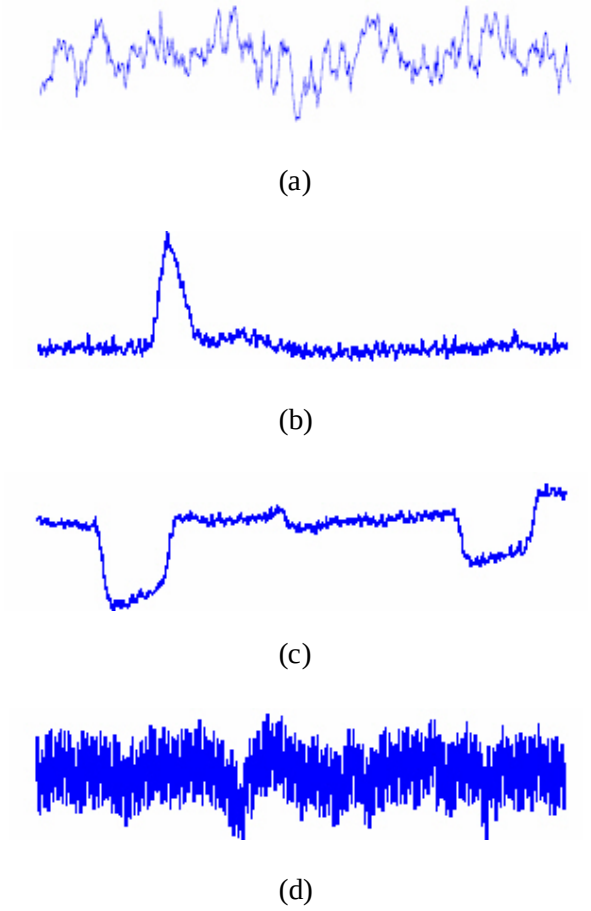

(a)

(b)

(c)

(d)

Figure 1.1 EEG signal and artifacts (a) Clean EEG signal (b) Eye blink(c) Eye movement (d) 50Hz noise

The inverse problem that reconstructs the electric sources in the brain from the potentials measured on the scalp, generally termed EEG inverse problem has been an important topic in electrophysiology for a long time. There are two different kinds of approaches to solve this inverse problem. The first kinds of approaches are based on dipole model, assuming one or multiple current dipoles to represent the electric sources, and trying to determine the location or amplitude of these dipoles. The second kineds of approaches employ distributed source model and estimate the current distribution in the brain, such as Low Resolution Electromagnetic Tomography (LORETA. The EEG inverse problem is well known for its indetermination. Moreover, the volume conductor characteristics of brain makes all of

the signals be compounded together, thus the EEG signals are compounded with external and internal noises and artifacts and uncorrelated brain electric activities. The external noises and artifacts may invalidate the inverse models if not correctly removed. The irrelevant brain electric activities make the inverse problem much more difficult as the number of multiple current dipoles cannot be determined for the dipole model. Although the LORETA does not need to assume the number of the multiple current dipoles, it fails to discriminate several different brain electric activities with nearby active areas, because of its low spatial resolution. Many methods are used in the pre-processing before solving the inverse problem(Du, Leong,1994; Larsen and Prinz, 1991; Noda,1989). Digital and analog filters are widely used to remove the noise and artifacts from the EEG signal. The choice of the parameters of the filters is based on the known characteristics of EEG signals, artifacts and noise. However, in real case, this condition can not be always met. The EEG signals of concerned brain electric activity are often interfered by many unknown or unexpected noise and EEG signals of irrelevant brain electric activities; moreover in some case, the characteristic of EEG signals of concerned brain electric activity is unknown neither. A widely used non parameter method in the research of Event-Related-Potential (ERP) is to filter out all kinds of noise and uncorrelated brain electric signals by averaging a large number of time-locked EEG trials. However, in the actual EEG measurement for brain activities which are spontaneous rather then event-related, such as epilepsy, ERP cannot be applied and thus the original LORETA can not be used.

For testing some EEG signal processing methods, such as Independent Component Analysis (ICA) for EEG signal separation, accurate information of the source signals is necessary. However, EEG signals are complicated and compounded with

environmental noise and unexpected artifacts. Moreover because of the volume conductor characteristic of brain the original signals are unknown. A testing platform that provides a real experimental environment is necessary and needed.

1.2 Research objectives

The first objective of this research was to develop a novel testing platform which can be easily acquired and is very similar to the human brain to verify various kinds of EEG signal processing methods, especially ICA for the decomposition of mixed signals on the head.

The second objective of this research was to automatically remove two major kinds of artifacts in EEG signals, ECG and ocular artifacts using ICA.

The third objective of this research was to locate specific brain activity in the brain from single-trial EEG signals.

Chapter 2

LITERITURE REVIEW

2.1 Previous work on ECG artifact removal

The ECG contamination may vary widely in intensity from subject to subject and even between epochs for a given subject.

Recording techniques such as balancing resistors and reference electrode placement (montage), help to minimize ECG signal, usually the references are located at the two earlobes. However, the montage is very sensitive to the dissymmetry of the distribution of ECG signals on the scalp. Although the strength of ECG signals does not obviously change across the EEG channels, the remnant of ECG artifact sometime is considerably large.

Thus techniques to eliminate the ECG signal have been proposed (Barlow and Dubinsky 1980; Ishiyama el al. 1982; Nakamura and Shibasaki 1987). These elimination techniques employ a subtraction of the average ECG from the EEG to construct a clean EEG record. Subtraction methods suffer from both the need to record a separate ECG channel and the inability to cope with a waxing and waning ECG contaminant.

The use of robust filters-smothers to eliminate ECG contamination was introduced to cope with these problems (Larsen and Prinz, 1991). These filter-smoothers do not require a separate channel of ECG information. In this kind of procedure, ECG artifacts are considered as additive outliners and the real EEG signal is obtained by a

robust A-R model algorithm. However, not only ECG artifacts are additive outliners in the A-R model, any suddenly appearing peaks may be additive outliners such as event related potentials (ERP). Thus, this technique can lead over correction. It was reported that by using Independent Component Analysis (ICA), ECG artifacts can be successfully removed without any over correction (Wei, Gotman, 2002). But these algorithms still need visual search for ECG artifact component. Thus they can not be used in online processing.

2.2 Previous work on Ocular artifacts

Among the many sources of artifacts in EEG studies, eye activity plays a dominant role. The need of ocular artifacts correction has been shown in the past, and several methods have been introduced (Brunia et al, 1989 and Jervis et al. 1988).

The simplest and actually most common eye artifacts correction method is rejection. It is based on discarding portions of EEG that correspond to EOG channel(s) containing attributes (e.g. amplitude peak, variance and slope) that exceed a determined criterion threshold (Barlow, 1979 and Verleger, 1993). However, the rejection method may lead to a significant loss of data, as well as lead to the portions used not being representative of the study made. This is particularly important when the brain signals of interest occur near/during strong eye activity, as happens for example in visual tracking experiments. Another problem associated with the rejection technique is that one may be unable to identify all eye activity beforehand, rejecting only the small portion that one can see, and considering artifact-free what is in fact only artifact-reduced. This may lead to wrong appreciation of the signals observed.

To reduce the presence of eye activity in EEG measurements, the subject is often asked to avoid blinking, fix the eyes on a target, or restrict the blinking at particular times. The effectiveness of this eye fixation method can be questionable, especially in studies of children and of psychiatric or neurological patients, who are not fully co-operative. Thus it may be difficult to collect a sufficient amount of artifact-free data. Besides, this requirement constitutes a secondary task, leading to reduced amplitudes in the task of interest (Weerts and Lang, 1973; Verleger, 1991).

A third class of methods, that could be called EOG subtracting methods, bases its action on the assumption that the measured EEG is a linear combination of true EEG and ocular artifact. Accepting that one or more EOG derivations well represent all eye activity, a correction is proposed by subtraction of a regressed portion of this signal throughout the EEG (Gratton et al., 1983). Time-domain and Frequency-domain regression methods are popular in EOG artifact removal. Time-domain regression methods assume that propagation of ocular potentials is volume conducted and frequency independent and without any time delay. The frequency-domain regression methods consider the medium through which the EOG activity is conducted to a scalp location a linear filter. This means for example that some frequencies can be attenuated more than others. In the time domain the relation between the actual EOG activity (denoted by $VEOG$) and the EOG artifact measured at a given scalp location, (denoted by $Veog$) can be then described as follows:

$$Veog_i(t) = \sum_{k=1}^{M} VEOG_i(t-k)\, p(k)$$

t=1, 2, 3, …, N, k=0, 1,2 ,..., M, M<N-1, (2.1)

In which i stands for successive trials (time over the experiment) and *t* for time in each trial, $p(k)$ is a series of weighted attenuation factors, namely the filter or system characteristics. The solution of this linear filter implicates that *Veog* is not only dependent on *VEOG*, but also on sample points in the past t - k. This means that the artifact *Veog* on the EEG can be deformed but remains linearly related to the EOG. (Woestenburg, et al 1982). There are disputes about the advantages of the frequency-domain regression over the time-domain regression, as it was reported that in reality the frequency dependence does not seem to be very pronounced. (Kenemans et al, 1991; Croft and Barry, 2000) However, neither time nor frequency techniques take into account the propagation of brain signals into recorded EOG. Thus a portion of relevant EEG signal is always cancelled out along with the EOG artifact. (Jervis et al, 1989).

Berg and Scherg (1994) have introduced another approach for eye artifact correction, a model based on multiple source eye analysis. In this MSEC (multiple source eye correction) approach, ocular artifact correction is performed by subtracting source waveforms defined by the eye activity, rather than proportions of the resulting EOG signals. The source waveforms are calculated from the EEG signal, together with topographic estimations of the propagation of eye activity throughout the head. This method results in considerable eye artifact suppression, but contains some basic restrictions. First, to perform this type of correction one has to choose a set of calibrating data containing eye activity that goes well above the background signals (in this context, the EEG). As stated above, this requirement may be difficult to fulfill. Second, the technique assumes orthogonality of the source vectors, that are a function of the location and orientation of each source, and of some head parameters. It is

possible that this solution represents a good approximation to the real conditions, but some further improvements may be necessary, like some independent considerations between each source and the background EEG. Signal-space projection method (Huotilainen et al, 1995) is used to identify and remove eye-blink artifacts, with much success. This approach, like that of Berg and Scherg (1994) requires either a prior modelling of the production of the artifact, or a considerable amount of data where the artifact's amplitude is much higher then the EEG or MEG under study. These requirements, as stated above, may be difficult to fulfill.

The adaptive filters are widely used in EOG artifact removal. One typical application of adaptive filtering is the interference cancellation by using the available reference to the interference. An adaptive eye artifact canceller is given in Fig 2.1 Adaptive filters are especially suitable for non-stationary signals such as the EEG.

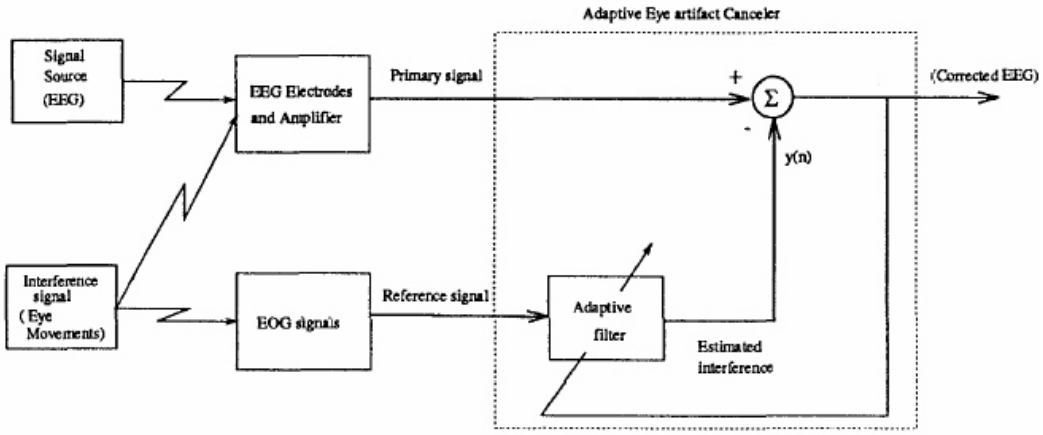

Figure 2.1 Adaptive filter eye artifact canceller

The essential assumption for an adaptive interference canceller is that the reference signal is uncorrelated with the desired signal. Otherwise, over correction will occur.

Unfortunately, the undesired correlations often exist due to the dc offset drift in the reference and the EEG signals. Slow cognitive potentials and head or body movement artifacts are often responsible for the dc offset drift. Quite a few on-line dc drift removal algorithms have been proposed in various contexts. All dc detrenders are essentially high-pass filters. Applying dc drift removal algorithms will inevitably have effects on the slow cognitive potentials. Since the slow potentials are important to many EEG studies, a dc detrender can not be used in these situations. Undesired correlations are the traditional difficulty in the adaptive filtering theory, and there are no general solutions to the problem. All feasible solutions are problem specific (Du, Leong and Gevins, 1994).

Time-frequency analysis has been introduced into the artifact removal. Wavelet based techniques for EOG artifacts removal have been proposed recently (Venkata Ramanan, 2004). Wavelet transforms are used to analyze time varying, non-stationary signals, and EEG falls into these category of signals. The ability of wavelet analysis to accurately decompose EEG into specific time and frequency components leads to several analysis applications and one among them is denoising. EEG signals have frequency content that varies as a function of time and recording sites on the scalp. Hence wavelet techniques can optimize the analysis of such signals by providing excellent joint time-frequency resolution, which is not possible with Fourier Transform. In contrast to Short Time Fourier Transform (STFT), wavelet transform adapts the window size according to the frequency. . In EEG data sets, there may be some specific components or events that may help the clinicians in diagnosis. They may tend to be transient (localized in time), prominent over certain scalp regions (localized in space) and restricted to certain ranges of temporal and spatial frequencies

(localized in scale). Wavelet analysis provides flexible control over the resolution with which neuroelectric components and events are localized in time, space, and scale. However the choice of value of wavelet coefficients threshold for de-noising is quite experiential. The general assumption of wavelet based de-nosing techniques is that the artifacts such as (heartbeat and EOG artifacts) are much stronger (10-100 times) than EEG signal. So the EEG signal can be considered as "noise" compared with artifacts and can be filtered out by setting a cut-off threshold from the wavelet coefficients of the recorded signal and then get the "pure" artifacts. The reconstructed EEG signals are obtained by subtracting the pure artifacts from the recoded signals. However, this assumption is not always true as the EOG artifacts decrease rapidly when propagating from forehead to occipital area. In the occipital channels the EOG artifacts are comparable with the EEG signal. In these channels, the EEG signal can not be considered as noise-like compared to EOG signal.

Inspired by the non-linearity of signal processing in the human brain, Rao and Reddy (1995) introduced a non-linear on-line method to enhance the EEG signals in the presence of ocular artifacts. Their method, using the recursive least squares based on the second-order Volterra filter, has shown good performance, but its non-linearity is still too limited, as it stops at second order statistics (variances and covariances). Mathematical and experimental work proves that higher order statistics may be needed to separate independent signals (Karhunen, 1996; Hyvarinen and Oja, 1997; Karhunen et al.,1997). Makeig et al. (1996) have recently introduced a comparable application of the independent component analysis (ICA) to EEG signals. Using ICA to separate brain activity from eye artifacts, based on the assumption that the brain and eye activities are anatomically and physiologically separate processes, and that

their independence is reflected in the statistical relation between the electrical signals generated by those processes. Even if no limitation seems to exist on the type of artifact that can be extracted, the fact that the ocular ones are the most representative justify their choice as illustration of the method. Like the application in ECG artifact removal, this method still needs visual search for EOG artifact component.

2.3 The EEG source reconstruction

The inverse problem of EEG is defined as the estimation of the distribution of electromotive force (EMF) in the brain from EEG by mathematical manipulations. As is well known, the solution to the inverse problem is not unique, since there exist silent EMF distributions that do not generate any electric at all outside the closed surface involving them (Rush, 1975). This difficulty is usually circumvented by making use of some simplified models for the EMFs such as multipoles, moving dipoles, multiple fixed dipoles, distributed source distribution and so on: the parameters of these models can be determined uniquely by fitting the forward solution to the measured EEG.

Depending on the models for the EMF distribution, various methods have been proposed to solve the inverse problems: equivalent dipole method (Musha and Okamoto, 1999), BESA (Scherg and Picton, 1991), MUSIC (Mosher and Leahy, 1998), LORETA (Pascual-Marqui et al., 1994) to name a few of the major ones. The equivalent dipole method is based on the moving dipole model. In this method EMF sources in the brain are approximated by a small number of current dipoles, and their locations and moments are estimated by fitting the EEG generated by them to the measured ones. In BESA (Brain Electric Source Analysis) and MUSIC (Multiple

Signal Classification), the locations of dipoles are assumed to be fixed during some time interval, and they are determined from the potential distributions measured repeatedly during that time interval. The LORETA source estimation approach is a kind of discrete and distributed source estimation. The source region is divided into grids. As the grids are dense enough, the dipole source can be considered to locate on each of the grid points. For a given orthogonal coordinate, the dipole sources with different strengths and directions can be expressed as the linear combination of the unit dipoles along x, y, z directions. N observing points were put on the scalp outside the source region. The relationship between the strength of the unit dipoles along the directions at each grid point and the potential at the observing points can be written as

$$\boldsymbol{v} = \boldsymbol{KJ} \tag{2.2}$$

where $\boldsymbol{J} = [j_1^T, j_2^T, \ldots j_M^T]^T$ is a 3M-vector comprised of the current densities j_i (3-vector) at M points with known locations within the brain volume; $\boldsymbol{v}$ is the N –vector comprised of measurements; $\boldsymbol{K}$ is the transfer matrix with $N \times 3M$ ranks. The transfer matrix of can be calculated by the numerical method, such as the finite-element method, however, the analytical expression is available for the sphere model of brain. The number of grids is usually greater than that of the observing points, that is 3M>N, so this simultaneous equation system is an underdetermined system, and it does not have a unique solution. The LORETA source estimation approach is to find out

$$\min_J \left\| BWJ \right\|^2 \text{ , under constraint: } \boldsymbol{v} = \boldsymbol{KJ} \tag{2.3}$$

where $\boldsymbol{B}$ is the discrete Laplacian operator $N \times 3M$ matrix. $\boldsymbol{W}$ is a diagonal matrix with, $w_{ii} = \left\| k_i \right\|^{-1}$ where k_i is the ith column of $\boldsymbol{K}$. If $\boldsymbol{W}$ is nonsingular, the unique solution of equ.2.3 is

$$J = W(KW)^{+} v \tag{2.4}$$

where $\boldsymbol{A}^{+}$ denotes the Moore–Penrose pseudoinverse of matrix. Thus a low resolution tomography is generated by this algorithm.

LORETA is famous for the generation the "smoothest" solution with the effect of depth properly considered. The distributed source model and the "smoothest" solution of LORETA have been adopted by many researchers because it is more physiologically realistic than the dipole model. The dipole model and the distributed source model are all based on the spatial distribution of the EEG potential, while the temporal characteristics of EEG signals are not fully considered. Moreover, all previous methods for EEG inverse problem are actually only available for event related potential (ERP) which is acquired from average of hundreds of time-locked EEG trials, and not available for single trial EEG. So they can not be used to locate the source of specific spontaneous brain activity.

2.4 The validation of EEG signal processing methods

There are two ways to validation of EEG signal processing methods.The first method is numeric simulation using simplified head models. Although several sophisticated head models have been developed which provide realistic head shapes (Cuffin, 1995), most commonly used models are multi-shell spherical models due to their simplicity in theoretical treatment and computation. These models consist of three to four concentric shells with different conductivity values representing the brain, skull,

cerebrospinal fluid (optional), and scalp (Rush and Driscoll, 1968; Cuffin and Cohen, 1979; Mingui, 1997; Pascual-Marqui, 1999). The choice of the head model is crucial as more simplified model requires less computation but loses more similarity to the real human head, while more sophisticated head models usually require large computation. Moreover, as the simulation methods only consider ideal situation in which the data is clean without any noise and artifacts, the ability of coping with noises and artifacts can not be tested by the numeric simulation way.

The second one is using implanted dipoles in epileptic patients undergoing presurgical intracerebral recordings (Cuffin et al 1991). The current dipoles are created by passing a weak (subthreshold) current through intracerebral electrodes implanted in the brains of epileptic patients for seizure monitoring. The locations of these dipoles are accurately known from roentgenographs. This method can provide totally realistic testing environment and most reliable results. However, implanting electrodes in the brain needs proper subjects and specific surgery, which are extremely inconvenient and not available for ordinary researchers.

2.5 Mathematical Background of Independent Component Analysis

Independent component analysis is a novel statistical technique which was developed in context with blind source separation (Jutten and Herault, 1991; Comon, 1994), in which case the original independent sources are assumed to be unknown, and yet to be separated from their weighted mixtures.

2.5.1 The Model

The basic data model used in defining (linear) ICA assumes that the observed n-dimensional data vector at time instant t, x(t) = [x1(t),…, xn(t)]T is given by

$$\mathbf{X}(t) = \sum_{i=1}^{m} \mathbf{a}_i \mathbf{s}_i(t) = \mathbf{A}\mathbf{s}(t) \tag{2.5}$$

where $\mathbf{s}(t) = [s_1(t), \ldots, s_m(t)]^T$ are m independent source signals with zero mean, which can be guaranteed by explicitly extracting the mean of each $x_i(t)$ without loss of generality, and $\mathbf{A} = [\mathbf{a_1}, \ldots, \mathbf{a_m}]$ is a constant mixing matrix which is a function of the location of the sources, the positioning in an EEG recording, the shape and the conductivity distribution of the brain as a volume conductor(Vigario, 1997). As in the general blind signal separation problem, **A** is assumed to be an n×m matrix of full rank (there are at least as many mixtures as the number of independent sources, i.e. n > m). In addition, although **A** is unknown, we assume it to be constant, or semi-constant (preserving local constancy) in order to perform ICA.

If W denotes the inverse or pseudo-inverse of A, the problem can be redefined equivalently as to find the separating matrix W that satisfies

$$\mathbf{s}(t) = \mathbf{W}\mathbf{x}(t) \tag{2.6}$$

2.5.2 The ICA algorithm

It has been documented that the preprocessing the input data (mixtures) by whitening can significantly ease the separation of the source signals (Karhunen et al., 1997). Therefore, in the first step, we implement standard principal component analysis (PCA) for whitening **x**. It can be shown in the compact form (noting that we have now dropped the time index t):

$$\mathbf{v} = \mathbf{V}\mathbf{x} \tag{2.7}$$

where $E\{\mathbf{v}\mathbf{v}^T\} = \boldsymbol{I}$ with $\boldsymbol{I}$ denotes the unit matrix. The whitening matrix $\mathbf{V}$ is given by

$$\mathbf{V} = \mathbf{D}^{-1/2}\mathbf{E}^T \tag{2.8}$$

where $\mathbf{D} = \mathrm{diag}[\lambda_1, \ldots, \lambda_m]$ is a diagonal matrix with the eigenvalues of covariance matrix $E\{\mathbf{x}_i\mathbf{x}_i^T\}$ as its diagonal elements, and $\mathbf{E}$ is a matrix with the corresponding eigenvectors as its columns.

The key to estimating the independent components from their mixtures by using ICA is non-Gaussianity. Intuitively speaking, maximizing the norm of this kurtosis leads to the separation of one non-Gaussian source from the observed mixtures. In our algorithm, non-Gaussianity is measured by the classical fourth-order cumulant or kurtosis. Consider $\mathbf{y} = \mathbf{w}^T\mathbf{v}$, with $\|\mathbf{w}\| = 1$, kurtosis is calculated by

$$kurt(\mathbf{y}) = E\{(\mathbf{y})^4\} - 3[E\{(\mathbf{y})^2\}]^2 \tag{2.9}$$

where operator E denotes the mathematical expectation.

Then the FastICA fixed-point algorithm based on gradient descent searching (Hyvarinen, 1999; Hyvarinen and Oja, 2000) is used to search the expectation maximization. As a result, rows of the separating matrix $\mathbf{W}$ and corresponding independent sources are identified one by one, up to a maximum of m. The basic steps of this efficient algorithm are as follows:

1. Choose initial vector w_0 randomly (iteration step l=0).
2. Let $\mathbf{w}_l = E\{\mathbf{v}(\mathbf{w}_{l-1}^T\mathbf{v})^3\} - 3\mathbf{w}_{l-1}$.
3. Let $\mathbf{w}_l = \mathbf{w}_l / \|\mathbf{w}_l\|$.

If stop criterion has not been satisfied, go back to step 2

Due to the cubic convergence of the algorithm (HyvLdnen and Oja, 1997a), the solution is typically found in less than 15 iterations.

Chapter 3

VOLUME CONDUCTOR PLATFORM FOR VALIDATION OF EEG SIGNAL PROCESSING ALGORITHMS

3.1 The volume conductor simulation platform

In this study, a volume conductor platform method using real volume conductors structurally similar to the human head for validation of EEG signal processing method by simulation was proposed. As one of such cases, a watermelon volume conductor simulation platform has been developed. It has been found that watermelon has some physical characters very similar to the human head. Firstly, a watermelon and a human head are both spherical volume conductors. Secondly, they are both composite of different layers with materials of different electrical resistances, as shown in Fig. 3.1 (a) and (b). In a human head, the average resistance of the scalp is about 2.22 Ωm, the average resistance of the skull is about 177Ωm, and the brain is about 2.22Ωm. In a watermelon, the average resistance of the peel is about 13kΩm, the average resistance of the white part of the flesh is about 186Ωm, and the red part is about 73Ωm. Although the values are different, the fundamental structural features are the same. These common features make watermelon an ideal model platform for simulation of the electric activity of the human head. By installing electric current dipoles in the watermelon and controlling the amplitudes and frequencies of the currents, the electric activity of a human head can be simulated. By placing EEG electrodes on the surface of the watermelon, the potentials on the watermelon surface can be measured in the same way as scalp EEG acquisition. The significant advantage of such a volume conductor simulation platform is that for specific measured EEG

data, the precise information of the corresponding electric activities in the volume conductor is known. This can be used to conduct accurate validation of many EEG signal processing methods, such as the ICA and special power mapping, as shown in the following sections.

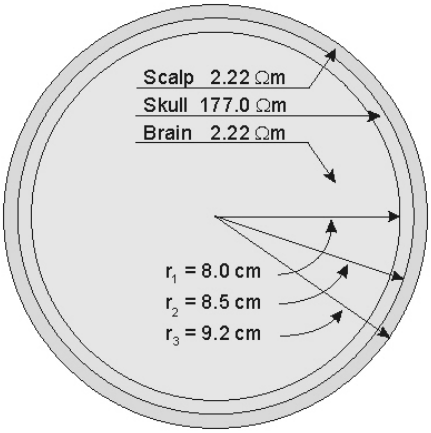

(a)

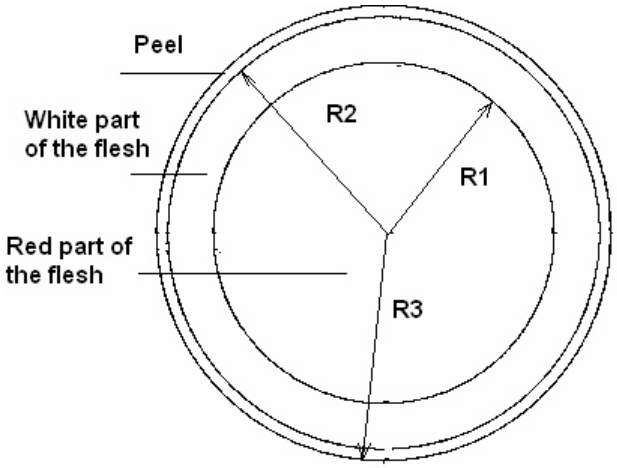

(b)

Figure 3.1 Models of human brain and watermelon
(a) Concentric spherical head model by Rush and Driscoll (1969). The model contains a region for the brain, scalp, and skull, each of which is considered to be homogeneous. (b) Concentric spherical structure of watermelon

3.2 Experiment Setup

In order to show how the proposed volume conductor brain activity simulation platform serves the purposes, experiments have been conducted. A watermelon of diameter 165 mm (close to the size of human head) was used for the volume conductor body. Six spinal electrodes were inserted into different part of the watermelon, forming three dipole sources in the volume conductor. The simulated brain activity signals were generated by three function generators. The simulated signals were injected into the watermelon through the spinal electrodes. To model the dipole sources, every source consists of two electrodes, one connected to the function generator the other is connected to the ground. A total of 17 electrodes were attached on the surface of the watermelon, according to the 10-20 system, to receive the signals. All signals are measured and recorded using a commercial EEG machine (Mactronis). The overall setup is shown in Fig.3.2.

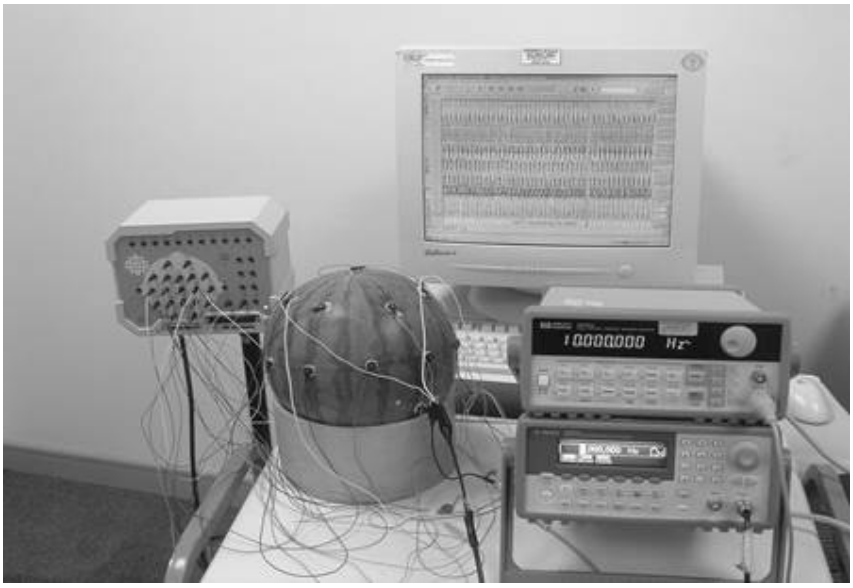

Figure3.2 Experimental setup for the validation of the volume conductor brain activity simulation platform

3.3 Results and discussions

3.3.1 Validation of ICA using the volume conductor brain activity simulation platform

ICA is a widely used method for blind signal separation. To test the validity of ICA in EEG signal decomposition, three signals, S1, S2…S3 of frequencies 4 Hz, 1 Hz and 8 Hz, respectively, were generated and injected into the watermelon through the spinal electrodes. The three groups of spinal electrodes were located at P4, Cz, T3, as shown in Fig. 3.3. The input source data, the raw data and separated signals are shown in Fig.3.4 and 3.5. Signals from the 17 channels on the surface of the watermelon were recorded, and then were separated into independent components by ICA. The separated independent components were validated by comparing the components with the original inputted signals. Because the ICA separated components have zero mean and unit variance, the original sources are normalized to zero-mean and unit variance, the mean root MSN between the ICA components and the corresponding normalized original sources were then computed, the mean root MSE of the separated signals was found to be 0.2, indicating a good accuracy in the signal separation.

3.3.2 Validation of spatial power mapping using the volume conductor brain activity simulation platform

In EEG measurement, spatial mapping is often used for identifying the location of the signal sources. The volume conductor platform can test the methodology of identification the source location easily. The same measured data obtained from the ICA validation as described in Section 3.3.2 were used for checking an EEG special power mapping method. The real locations of the three dipole sources generated by

the three groups of spinal electrodes were known at P4, Cz, and T3, respectively, as shown in Fig 3.3. Compared with the three source locations determined according to the spatial power mapping as shown in Fig 3.5, identified according to the frequency bands 1.5-2.5 Hz, 3.5-4.5 Hz, and 7.5-8.5 Hz of the dipole sources. The accuracy of the special mapping in terms of dipole source frequency and locations was validated by comparing the actual dipole sources and with the three maps. Comparing the 3 dipole sources and the 3 power maps, it was found that each of the maps corresponding to one of the three frequency bands shows only one peak, which has the location exactly the same as the location of the dipole source having the frequency within the band.

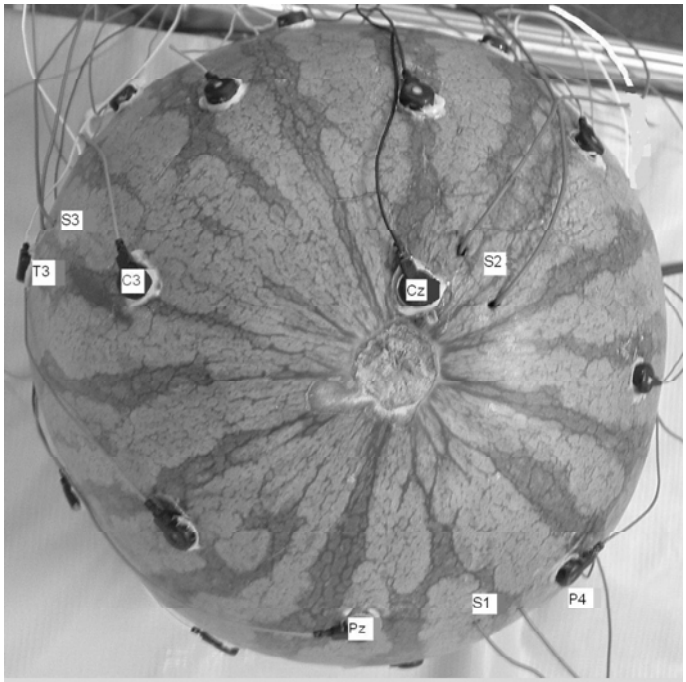

(a)

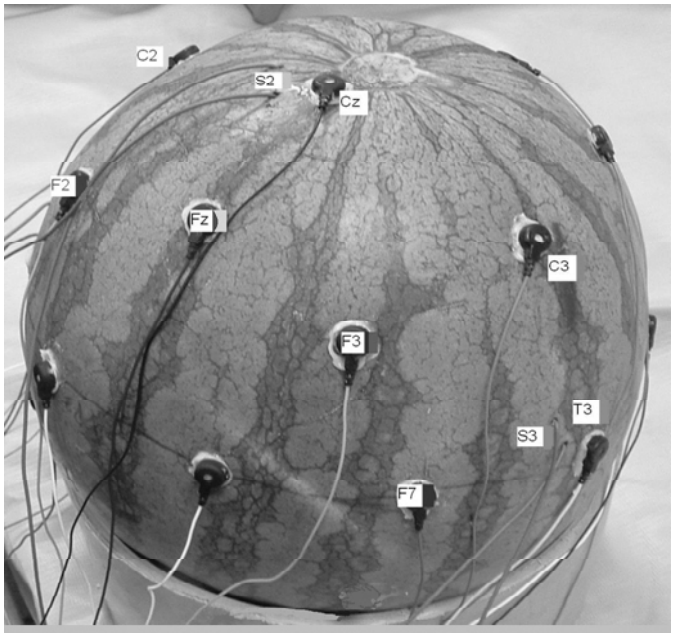

(b)

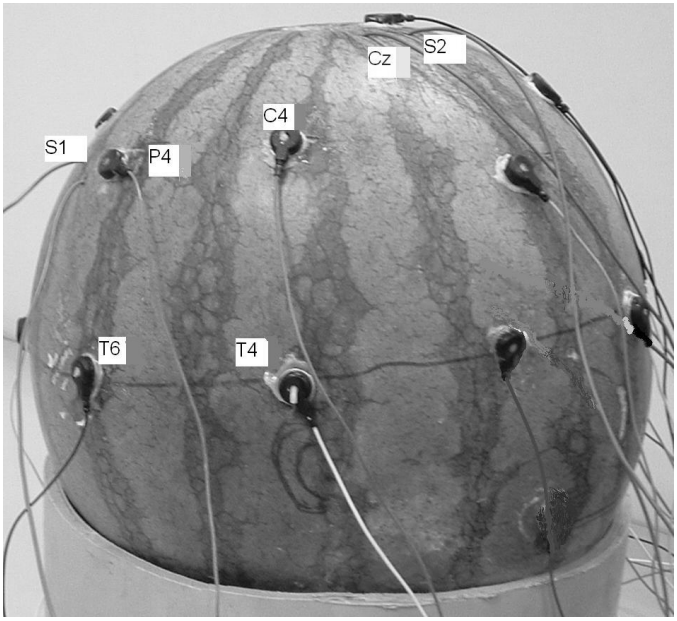

(c)

Figure 3.3The location of the sources. (a) Platform of source location (b) Left side view of source location(c) Right side view of source location

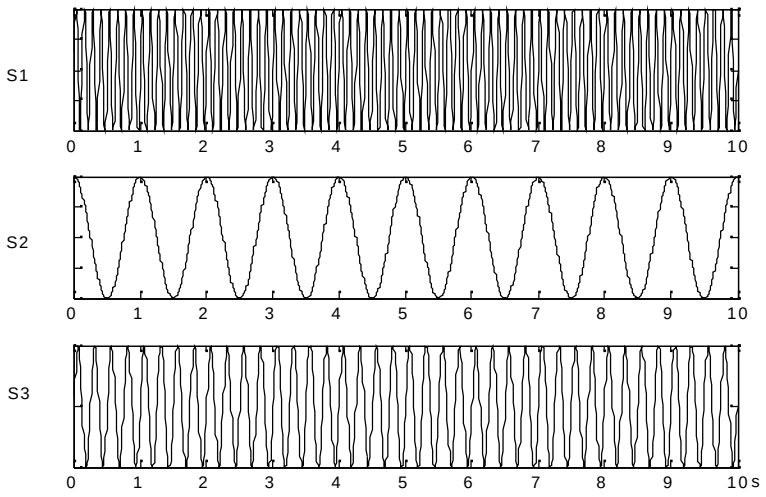
S1
S2
S3
0 1 2 3 4 5 6 7 8 9 10
0 1 2 3 4 5 6 7 8 9 10
0 1 2 3 4 5 6 7 8 9 10 s

(a)

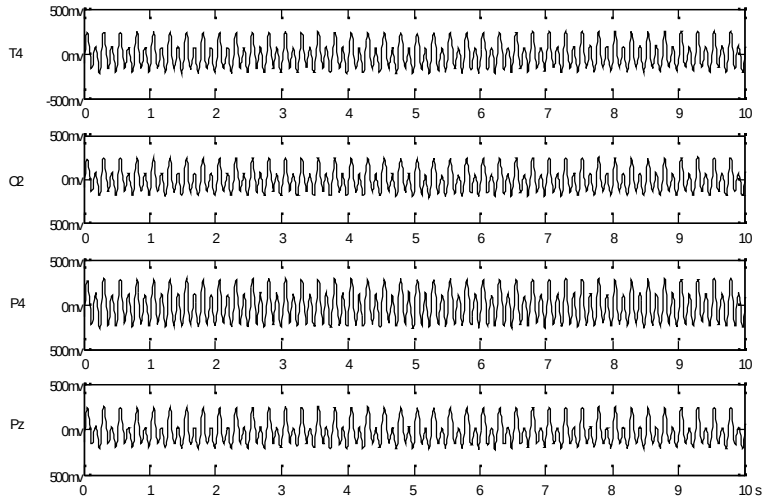
T4
O2
P4
Pz
500mv
0mv
-500mv
0 1 2 3 4 5 6 7 8 9 10
0 1 2 3 4 5 6 7 8 9 10 s

(b)

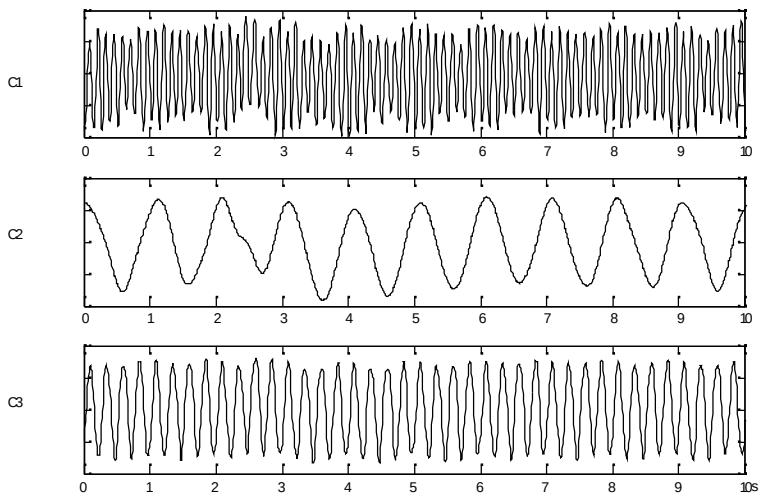

(c)

Figure 3.4 Result of ICA Experiment (a) ICA test for three sources. (a) Input source data. (b) Raw data of ICA testing experiment. (c) ICA components C1, C2 and C3 are separate sources, 8Hz, 1 Hz and 4 Hz sinuous waves.

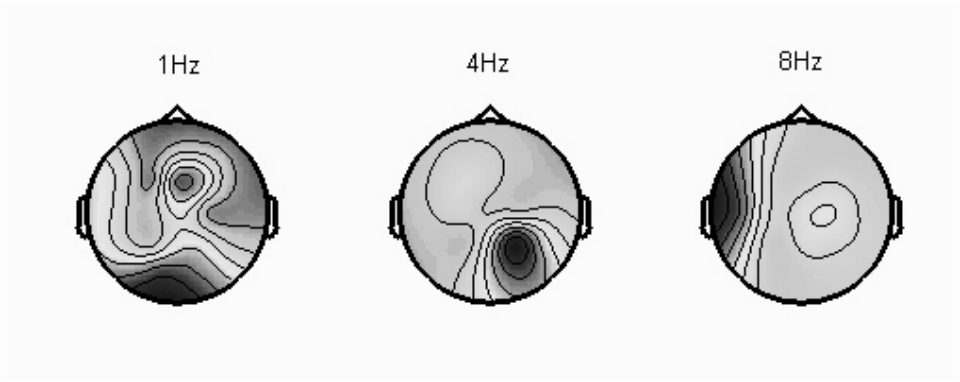

(a)

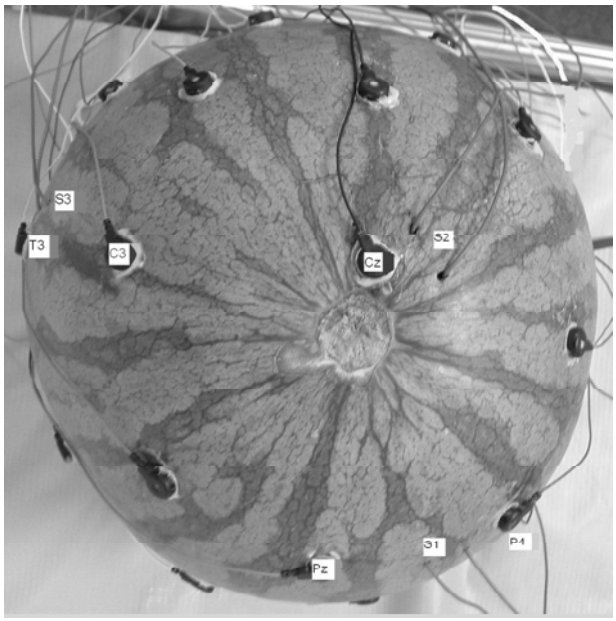

(b)

Figure 3.5 (a) Power spatial maps at three frequency bands. The maps are gray scaled, dark represents large amplitude. (b)The real source location on the watermelon

Chapter 4

ICA BASED AUTOMATIC ARTIFACT REMOVAL

4.1 Model of ECG artifact

Because the heart is far away from the head, the potentials of ECG artifact is almost the same everywhere on the scalp. After ICA decomposition, the entries of the coefficient map of the component corresponding to ECG artifact are expected to have the same amplitude. As the sources of brain activities are inside the brain and near the electrodes on the scalp, the entries of the coefficient map of the corresponding components are the function of the location of the sources and different with each other. Thus, this feature is unique for the identification of ECG components. Fig.4.1 shows the ICA components and coefficient maps of ECG component and brain activity components. It is shown that the coefficient map of ECG component is the same everywhere with out any change, while the coefficient map of brain activity component changes a lot from location to location.

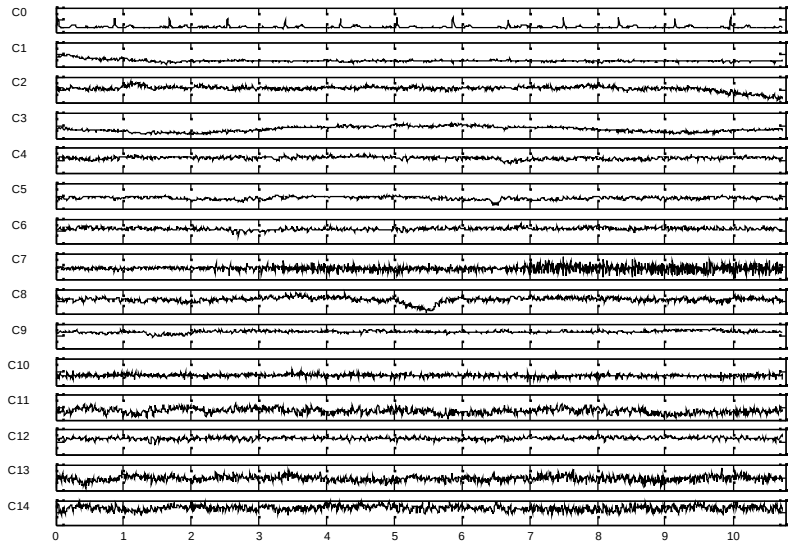

(a)

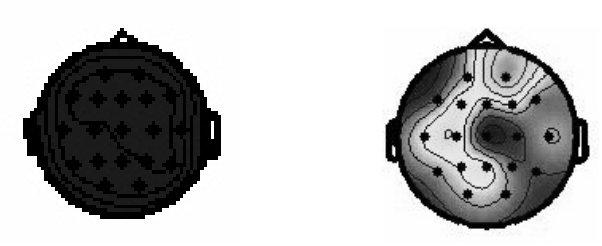

(b)

Figure 4.1: ICA components and coefficient maps. (a)Component C2 corresponds to some brain activity component C0 corresponds to the heartbeat artifacts (ECG). (b) The coefficient maps of components C0 and C2. The maps are gray scaled, dark represents large amplitude.

The numeric description of this feature is given by the normalized variance:

$$Var_n(\mathbf{a}_i) = Var(\mathbf{a}_i) / Mean(\mathbf{a}_i)^2 \qquad i = 1, 2, \ldots \mathrm{M} \tag{4.1}$$

$Var()$ denotes the variance of the entries of a vector, $Mean()$ denotes the mean of the entries of a vector, i stands for the ith components, M stands for the number of independent components of ICA.

Apparently, the coefficient vector of ECG component has the minimum normalized variance. The identification of ECG component can be realized by finding the component $\mathbf{s}^*$ of which coefficient vector $\mathbf{s}^*$, minimizes the $Var_n(\mathbf{a})$. It is easy and feasible if ICA can separate the ECG artifacts from brain activities. However, in case, ECG artifact is not separated from brain activities by ICA, this method will discard other components instead. So a more robust method is needed. When $Var_n(\mathbf{a}^*)$ exceeds a threshold c, the corresponding component is remained. The experiential value of c is 0.01.

4.2 Automatic ECG artifact removal algorithm

The algorithm for automatic ECG artifact removal is as follows:

(1) Decompose the original data **x** by ICA to get the components $\mathbf{s}_i$ and the coefficient vectors $\mathbf{a}_i$ of each component. Where i=1,2,…M , M is the number of the total ICA components

(2) Find the component **s*** of which the coefficient vector **a*** satisfies the conditions below:

$$Var_n(\mathbf{a}^*) = Var(\mathbf{a}^*) / Mean(\mathbf{a}^*)^2,$$

$$Var_n(\mathbf{a}^*) = \underset{i}{Min}(Var(\mathbf{a}_i) / Mean(\mathbf{a}_i)^2),$$

$$Var_n(\mathbf{a}^*) \le c,$$

(3) If $\mathbf{a}^*$ is found, correct the original data

$$\mathbf{X}_c(t) = \mathbf{X}(t) - \mathbf{a}^*\mathbf{s}^*(t)$$

60 3-second-long epochs of EEG data from 5 subjects were tested. The ECG artifacts were successfully separated and identified from 58 sections. The ICA could not separate ECG artifacts from 2 sections, and the ICA components were remained by the algorithm. Fig. 4.2 shows the result of automatic ECG artifact removal on one epoch of the EEG raw data. Table 4.1 shows the normalized variances of the ICA components

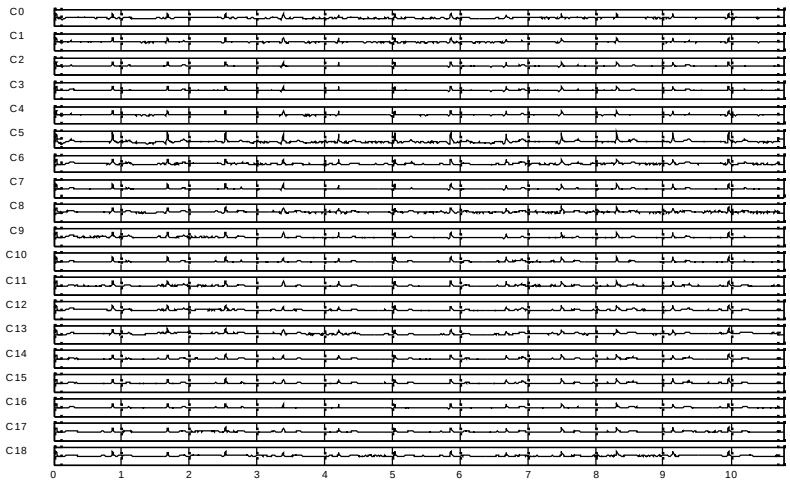
C0
C1
C2
C3
C4
C5
C6
C7
C8
C9
C10
C11
C12
C13
C14
C15
C16
C17
C18
0
1
2
3
4
5
6
7
8
9
10

(a)

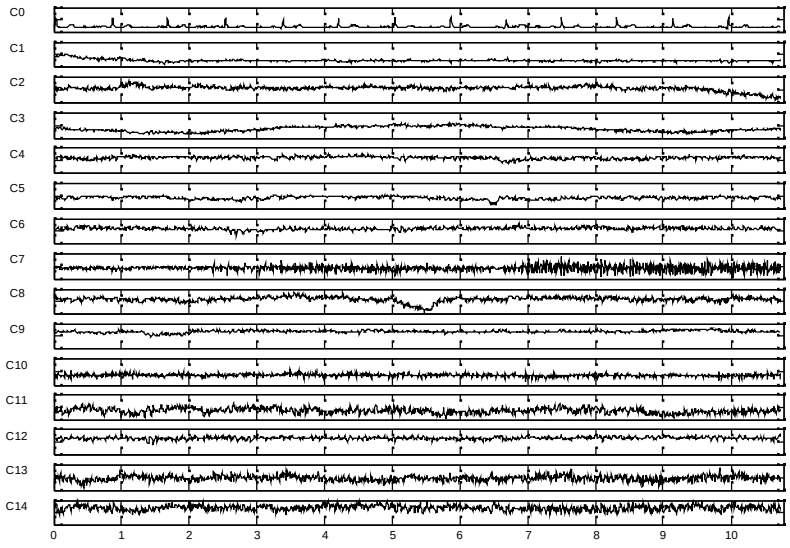
C0
C1
C2
C3
C4
C5
C6
C7
C8
C9
C10
C11
C12
C13
C14
0
1
2
3
4
5
6
7
8
9
10

(b)

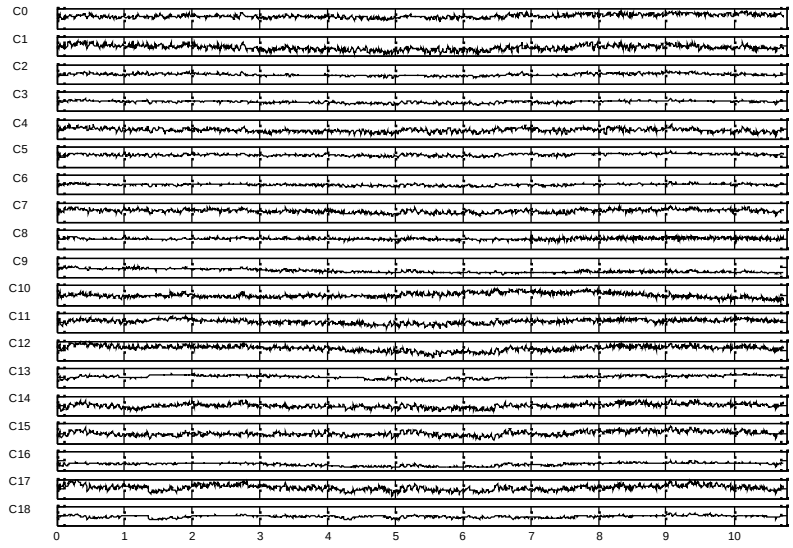

(c)

Figure 4.2 The ECG artifact removal. (a) the raw EEG data contaminated by ECG artifact. (b) Components decomposed by ICA (c) Corrected EEG

C0: 0.0005	C5: 15.0373	C10: 33.1776
C1: 1.2767	C6: 43.0366	C11: 16.0629
C2: 507.3110	C7: 191.0964	C12: 0.5863
C3: 753	C8: 6.5521	C13: 105.0777
C4: 3.2198	C9: 35.7737	C14: 26.0770

Minimum normalized variance: 0.0005

ECG component identified: C0

Table 4.1 Normalized variance of the ICA components

4.3 Model of Ocular Artifacts

There are two different originating phenomena for ocular potentials. There is a potential difference of about 100mv between a positively charged cornea and negative cornea of the human eye, thus forming an electrical dipole, so called cornea- retinal dipole. Firstly, the rotation of the eyeball results in changes of the electrical field across the skull. Secondly, eye blinks are usually not associated with ocular rotation. However, the eyelids pick up the positive potential as they slide over the cornea. This creates an electrical field that is also propagated through the skull.

The mechanism of origin and the direction of eye movements determine the resulting EOG wave shape. Vertical, horizontal and round eye movements usually result in square-shaped EOG waveforms, while blinks are spike-like waves.

The OA are large, transient slow waves. The eye moment artifacts typically occupy the lower frequency range; from 0Hz up to 6-7Hz. The eye blinking artifact can reach to alpha band (8-13Hz).

4.3.1 The correlation between EOG and ICA components corresponding to the Ocular Artifacts

The EOG is a reliable indicator of ocular movements and ocular eye movements are independent with brain activities, thus the ICA components corresponding to the OAs are expected to be highly correlated with EOG, while other components corresponding to the brain activities are expected to be uncorrelated with EOG. However the recorded EOG are corrupted by the EEG, the correlation between EOG and artifactual components is suppressed and the correlation between EOG and non-artifactual components is enhanced. Thus, it is necessary to remove EEG from the recorded EOG channel before identifying artifactual components by using correlation between EOG and ICA components.

4.3.2 Wavelets based de-nosing on recorded EOG

(1) Problem Statement

As previously mentioned, the recorded EOG is also contaminated by the EEG. It can be assumed that the recorded EOG is a superposition of the true EOG and some portion of EEG signal, thus we have:

$$EOG_{rec}(t) = EOG_{ture}(t) + k * EEG_{true}(t) \tag{4.2}$$

Where $EOG_{rec}(t)$ is the contaminated EOG, $EOG_{true}(t)$ is due to eye activities, and $k * EEG_{true}(t)$ is the propagated brain activities at the recording site.

The true EEG is a noise-like signal. We can not observe any clear patterns within it, nor can we simply correlate the particular underlying events with its waveform. Furthermore, in the awake, conscious state, neurons are firing in a more independent fashion. As a result of this resynchronization, the EEG signal is even more random-appearing.

(2) Wavelet Thresholding

The main statistic application of wavelet thresholding is a nonparametric estimation of the regression function f, based on observations s_i at time points t_i. The s_i observations are modeled as:

$$s_i = f(t_i) + \varepsilon_i, \quad i = 1, 2, ...N (N = 2^n) \tag{4.3}$$

Where ε_i are independent and identically distributed $N(0, \sigma^2)$ random variables (noises) at equally spaced time points t_i.

Due to the orthogonality of the wavelet transform, we are allowed to perform filter in the space of wavelet coefficient. The procedure for suppressing the noise involves i) finding the coefficients of the wavelet transform of $\{s_i\}$; ii) comparing each coefficient against an appropriate threshold; iii) keeping only those coefficients larger than the threshold; iv) applying an inverse wavelet transform to obtain an estimate of f.

The assumption is that large coefficients kept after thresholding belong to the function to be estimated, and those discarded belong to the noise. This is a fair assumption due to the good energy compaction of the wavelet transform. It is expected that some of the coefficients of the function might be discarded because they are of the same level as the noise coefficients. Thus, the performance of this technique depends on the proper choice of the wavelet filter that results in only a few nonzero function coefficients and the SNR, the lower SNR is, the more function coefficients will be of noise level and discarded. Fig. 4.3 and Fig. 4.4 clearly show how the noise energy influences the performance of wavelet de-noising. In our application, since the pure EOG is much higher than propagated EEG, the wavelet de-noising can perform well.

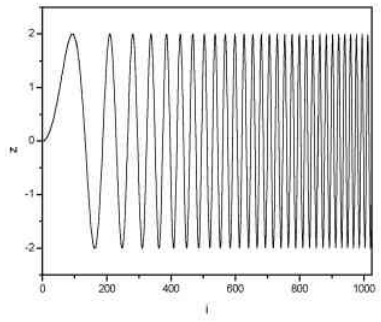

Figure 4.3 Original signal, the length is 1024 points

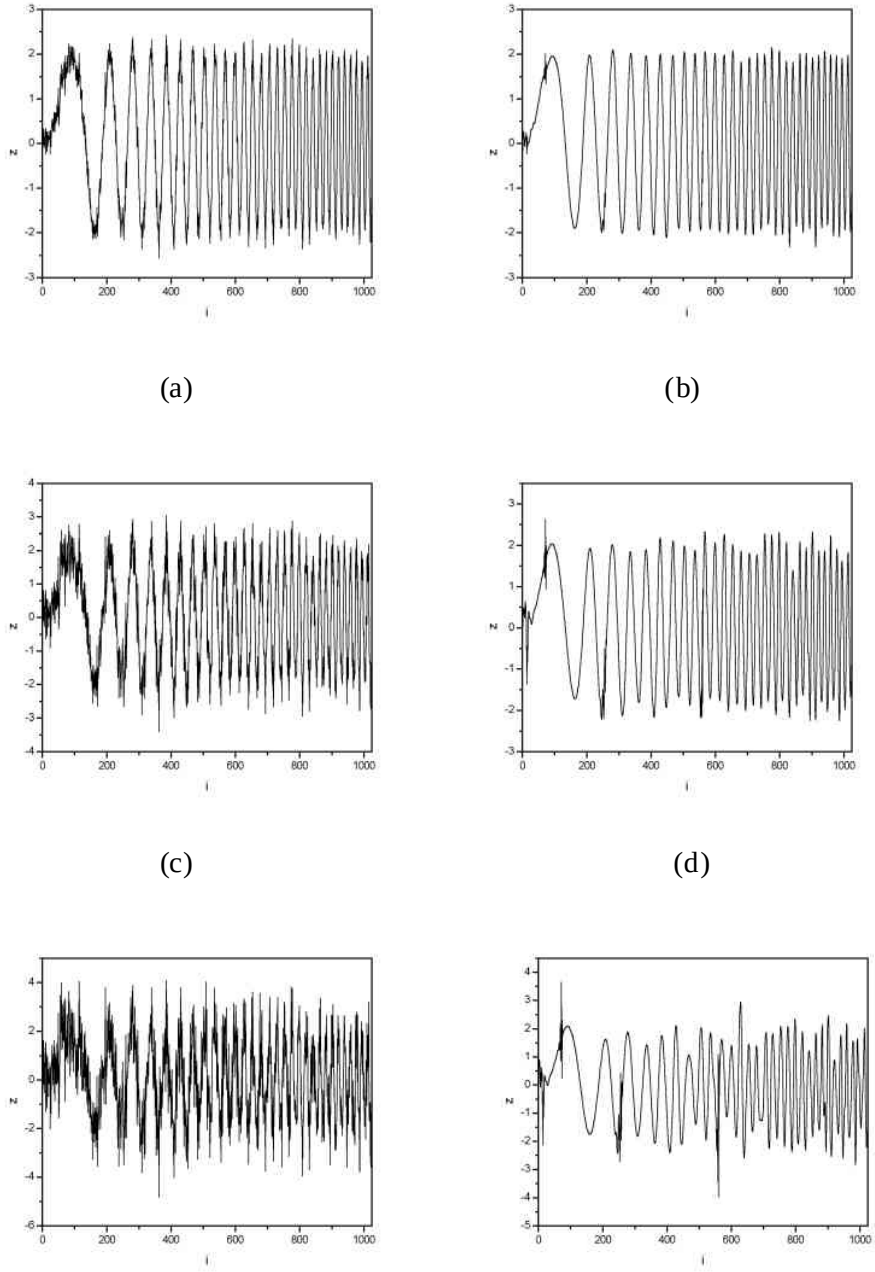

(a) (b)

(c) (d)

(e) (f)

Figure 4.4The performance of wavelet de-noising under different noise energy level

(a),(b) Gaussian noise with sigma=0.2 was added to the original signal. The waveform of the estimated signal by wavelet de-noising is the same as the original signal

(c),(d) Gaussian noise with sigma=0.5 was added to the original signal. The waveform of the estimated signal by wavelet de-noising is slightly distorted.

(e),(f) Gaussian noise with sigma=1 was added to the original signal. The waveform of the estimated signal by wavelet de-noising is serious distorted.

(3) Stationary Wavelet Transform

It is known that the classical DWT suffers a drawback: the DWT is not a time-invariant transform. This means that, even with periodic signal extension, the DWT of a translated version of a signal X is not, in general, the translated version of the DWT of X (Coifman and Donoho,1995).How to restore the translation invariance, which is a desirable property lost by the classical DWT.

The idea is to average some slightly different DWT, called ε-decimated DWT, to define the stationary wavelet transform (SWT). There is a restriction: we define the SWT only for signals of length divisible by 2^J, where J is the maximum decomposition level, and we use the DWT with periodic extension. The approximation and detail sequences at each level of decomposition are of the same length as the original sequence, rather than becoming shorter by a factor 2 as the level increases (Nason and Silverman, 1995).

The analysis is based on 960 point- long epoch of EOG signal (about 5.74 second, the signal was sampled at 167Hz), the same length as the EEG epoch that decomposed by ICA. Eye activity occupies the low frequency bands, from (0 up to 6-7 Hz) for eye movement artifacts, and between (8-13 Hz), excluding very low frequencies for the eye blink. Stationary Wavelet Transform (SWT) is used to decompose the recorded EEG into various frequency scales. SWT is chosen since it is time invariant and also it has better sampling rates in the low frequency bands, which produces smoother results. The decomposition level is restricted to five (0-2 Hz, 2-4 Hz, 4-8 Hz, 8-16 Hz,

16-32 Hz and 32-64 Hz), in order to have a reasonable computational complexity. The mother wavelet should be chosen in such a way that it better approximates and captures the artifacts in the noisy EEG signal. Coiflet 3 wavelet has been chosen as the basis function, since it resembles the shape of the eye blink artifact. This maximizes the amplitude of coefficients corresponding to the eye blink artifacts in the lowest band of the decomposition. It has turn out that it works properly as well for the eye movement artifacts as well.

In the proposed scheme, the following threshold was used for calculating the threshold limits:

$$T_k = mean(H_k) + 2 * std(H_k) \tag{4.4}$$

where H_k denotes the wavelet coefficients of kth level of decomposition.

Fig. 4.5 and Fig. 4.6 show the result of the de-nosing for a single epoch of eye blinking and eye rolling.

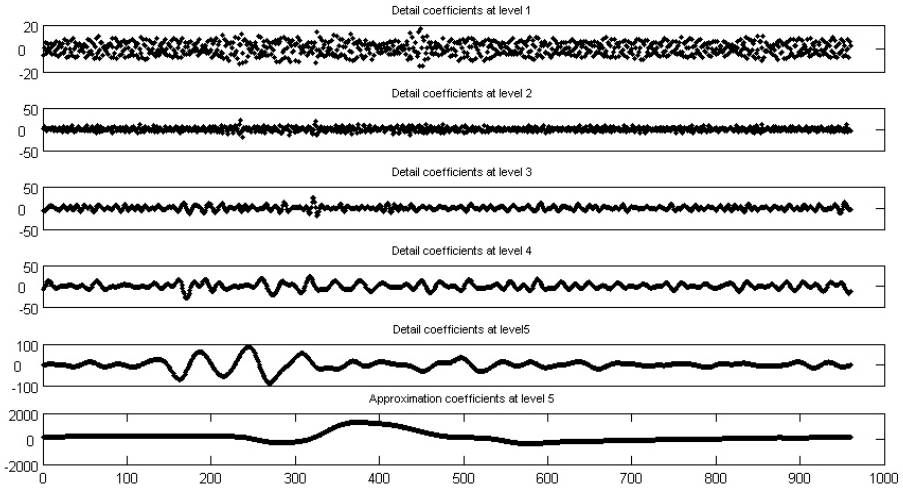

(a)

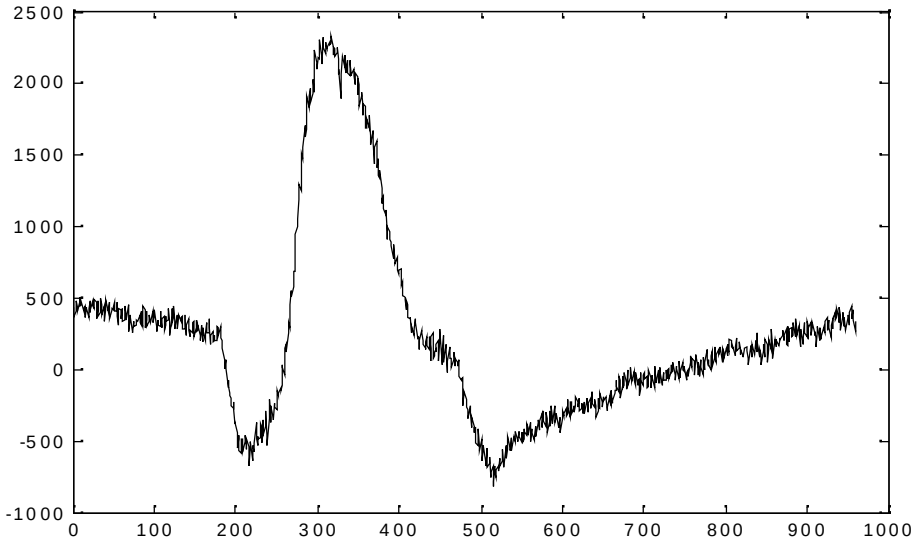

(b)

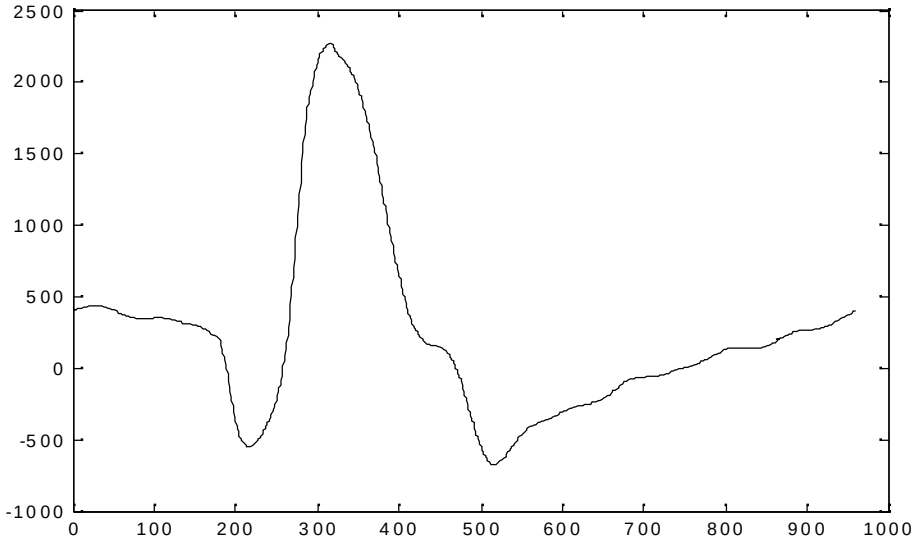

(c)

Figure 4.5 Wavelet De-noising for eye blinking (a)Stationary wavelet decomposition
of contaminated EEG (b) Contaminated EOG (c) corrected EOG

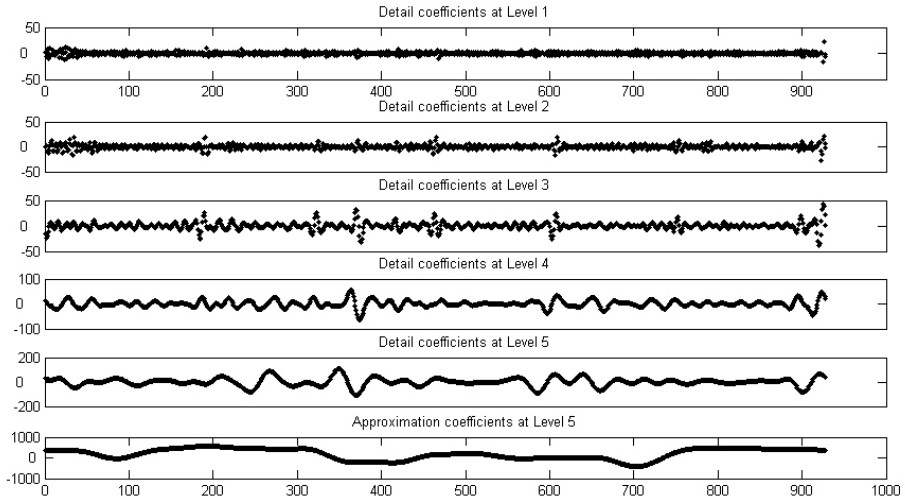
Detail coefficients at Level 1
Detail coefficients at Level 2
Detail coefficients at Level 3
Detail coefficients at Level 4
Detail coefficients at Level 5
Approximation coefficients at Level 5

(a)

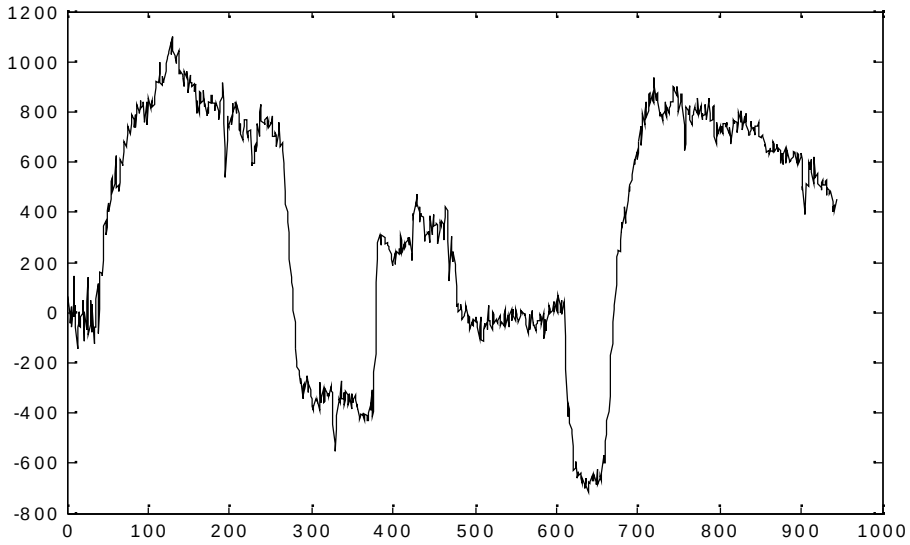

(b)

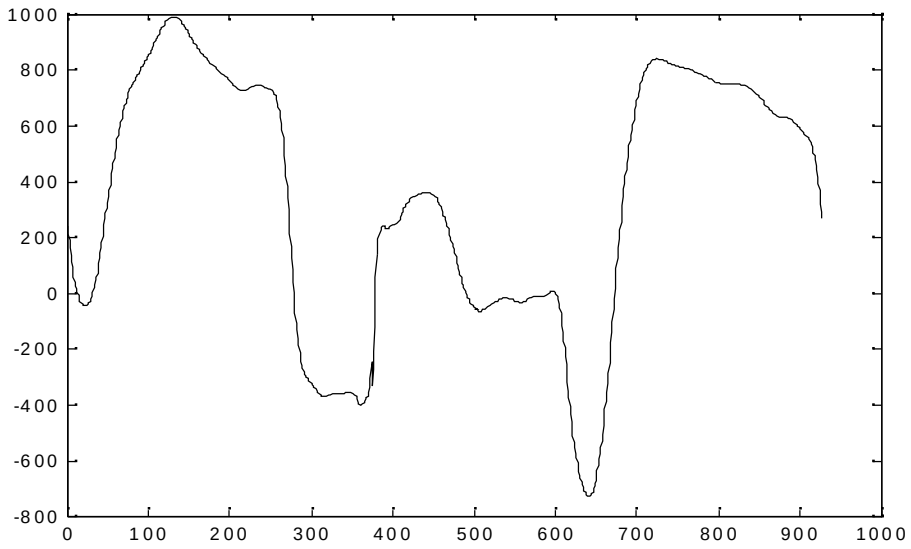

(c)

Figure 4.6 Wavelet De-noising for eye rolling (a) Stationary wavelet decomposition of contaminated EEG (b) Contaminated EOG (c) and corrected EOG

4.4 Automatic Ocular artifacts removal algorithm

The method has the following key steps:

1. Four EOG channels in addition to the international standard 10-20 system are used in the EEG measurement; the placement of the electrodes is shown in Fig.4.7:

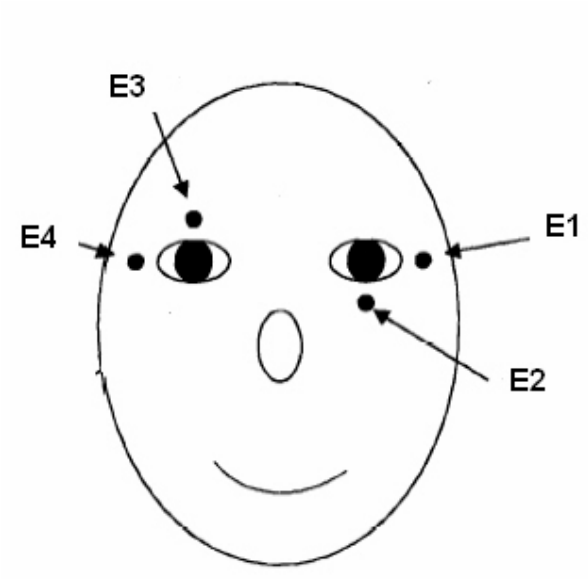

Figure 4.7 The electrode placement scheme

2. The EEG raw data is decomposed into a number of independent components by an Independent Component Analysis (ICA);

3. The portion of EEG in EOG is filtered out using a Stationary Wavelets Transform De-nosing (SWTD) method.

4. Each ICA component is regressed upon the two corrected EOG channels, and is identified as artifactual when the squared multiple correlation coefficient (R^2) exceeds a cutoff value.

5. Finally, the EOG components are corrected by the SWTD method and removed from the raw EEG data.

Fifty 5- second- long epochs of EEG and EOG signals are studied. The mean R^2 of un-artifact components is 0.2209 with variance σ^2 = 0.032 and the mean R^2 of artifact components is 0.74 with variance σ^2 =0.213. Thus 0.5 is reasonable value for cutoff. Fig.4.8 shows the results of this algorithm for a single epoch of contaminated EEG data. Table 4.2 shows the R^2 of each ICA components

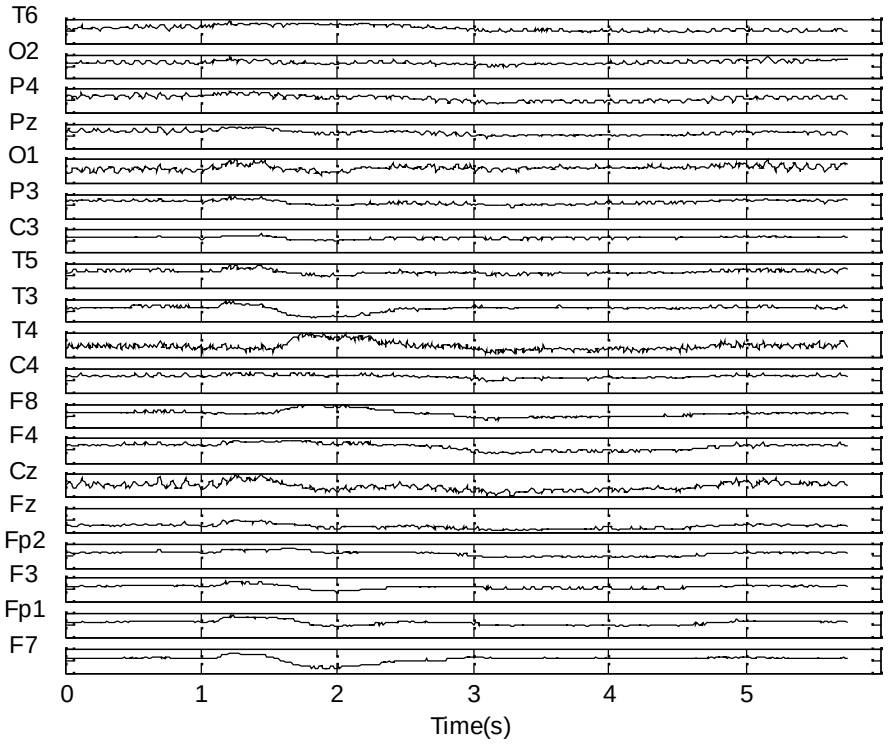
T6
O2
P4
Pz
O1
P3
C3
T5
T3
T4
C4
F8
F4
Cz
Fz
Fp2
F3
Fp1
F7
0
1
2
3
4
5
Time(s)

(a)

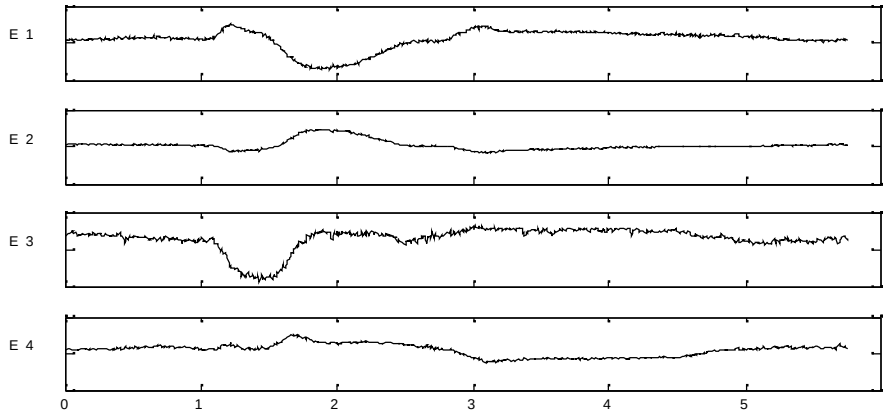
E 1
E 2
E 3
E 4
0
1
2
3
4
5

(b)

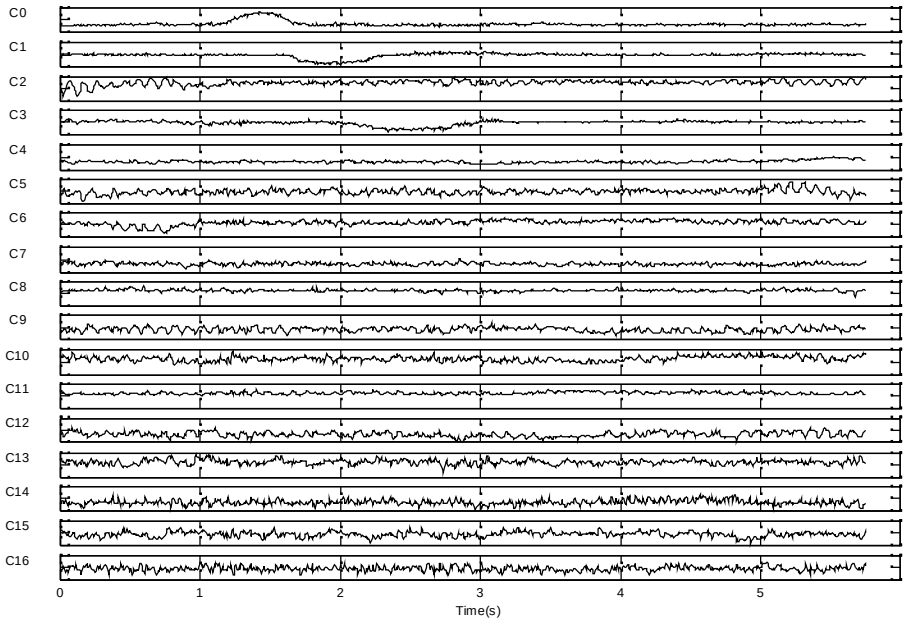
C0
C1
C2
C3
C4
C5
C6
C7
C8
C9
C10
C11
C12
C13
C14
C15
C16
0
1
2
3
4
5
Time(s)

(c)

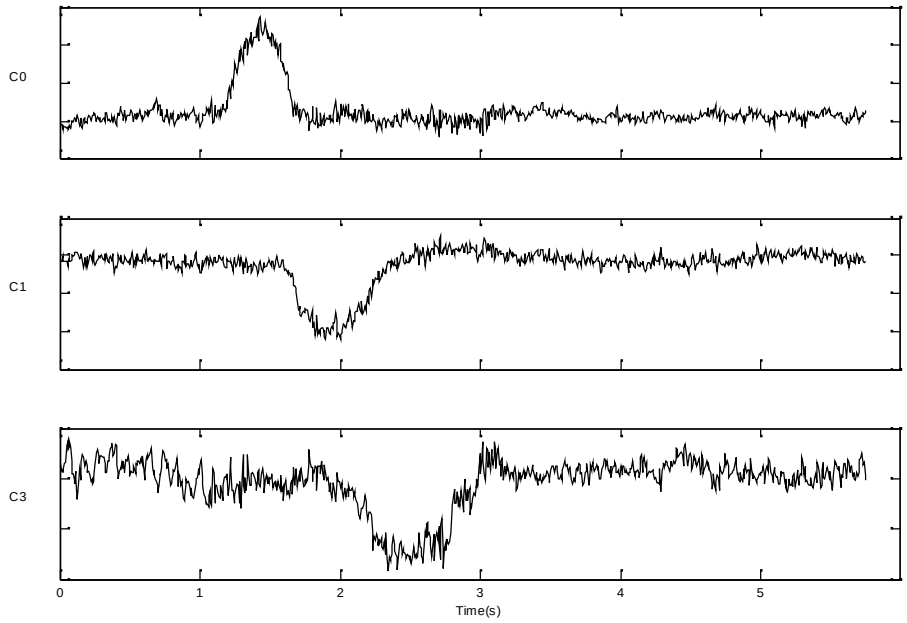
C0
C1
C3
0
1
2
3
4
5
Time(s)

(d)

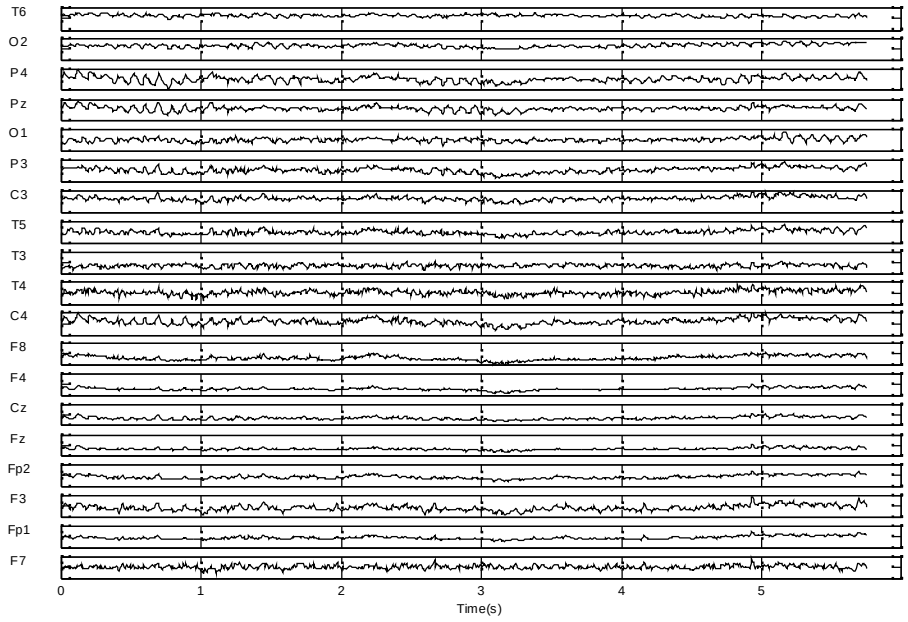

(e)

Figure 4.8 The result for a single epoch of contaminated EEG (a) Raw EEG data (b) Recorded EOG (c) ICA components of the raw EEG (d) The EOG artifactual components identified by the algorithm (e) Corrected EEG

C0: 0.9554	C5: 0.0267	C10: 0.1599	C15: 0.1786
C1: 0.9415	C6: 0.4482	C11: 0.3678	C16: 0.0519
C2: 0.1679	C7: 0.0949	C12: 0.2116	
C3: 0.5894	C8: 0.1766	C13: 0.0292	
C4: 0.1665	C9: 0.1445	C14: 0.1450	

EOG components identified: C0, C1, C3

Table 4.2 R^2 of the ICA components

The experiment results show that by applying automatic components selection algorithms, ICA can be used in on-line artifact removal. Although different artifacts

need different selection algorithms, the system can work effectively, as these algorithms take little running time compared with the ICA decomposition. Moreover, in some cases, some kinds of artifacts are considered as signal instead, thus moving different kinds of artifacts one by one can provide additional choice to decide whether the artifacts will be removed as noise or remained as useful information.

Chapter 5

ICA BASED LORETA FOR BRAIN ACTIVITY SOURCE LOCATING

5.1 The ICA-LORETA method

An algorithm combining ICA and LORETA is presented in this chapter. This algorithm is based on the basic assumption that the electric current sources (neurons) involved in specific brain electric activity are simultaneously and synchronously activated and independent of the sources of other uncorrelated brain electric activity. This assumption is supported by previous animal studies (Pascual-Marqui, R.D, et al 1994). Thus a linear model of the relation between the oscillation of the electric current sources and the measured EEG signals on the scalp can be developed. The discrete distributed source model at time instant ***t*** can be written as:

$$\boldsymbol{V(t) = KJ(t)+AN(t)} \tag{5.1}$$

where $\boldsymbol{J(t)} = [j_1(t)^T, j_2(t)^T, \ldots j_M(t)^T]^T$ is a $3M$-vector comprised of the current densities $j(t)$(3-vector) at M points with known locations within the brain volume; ***V(t)*** is the N –vector variable comprised of measurements; ***K*** is the transfer matrix with $N \times 3M$ ranks. $\boldsymbol{N(t)} = [N_1(t), \ldots, N_l(t)]^T$ are L independent noise sources out of brain volume contributing to the measurement on the scalp; ***A*** is the noise transfer matrix with rank $N \times L$. Assume there are l different brain activities occurring in the observing time period, each has an independent dynamic current source distribution $J_i(t)$, $i=1,2,\ldots l$; ***J(t)*** equals to the superposition of the l distributions:

$$\boldsymbol{J(t)} = \sum_{i=1}^{l} J_i(t) \tag{5.2}$$

According to the simultaneity and synchrony assumption, the J_i(t) can be rewritten as $\boldsymbol{J}_i\boldsymbol{S}_i$(t), where $\boldsymbol{J}_i = [j_{1i}^{T}, j_{2i}^{T}, \ldots j_{Mi}^{T}]^T$ is a 3M-vector comprising the variances of current densities j_i(t) in 3 directions (3-vector) at M points, S_i(t) is a temporal variable with unit variance and zero mean describing the simultaneous and synchronous temporal oscillation of the current densities, thus Eq. (5.1) can be rewritten as:

$$\boldsymbol{V(t) = BS(t) + AN(t)} \tag{5.3}$$

Where $\boldsymbol{B} = [\boldsymbol{KJ}_1, \boldsymbol{KJ}_2, \ldots \boldsymbol{KJ}_l]$ is the $N \times l$ matrix; $\boldsymbol{S(t)} = [S_1(t), S_2(t) \ldots S_l(t)]^T$ are l independent variables. Eq. (5.3) can be rewritten as the ICA linear model:

$$\boldsymbol{V(t) = [B, A]\,[S(t), N(t)]^T} \tag{5.4}$$

If $l + L \leq N$, the ICA algorithm can estimate $\boldsymbol{B}$ and $\boldsymbol{S(t)}$ from $\boldsymbol{V(t)}$. Suppose that the ith independent component is corresponding to the specific brain activity. Let $\overline{B_i}$ denote the estimation of $\boldsymbol{B}_i$ obtained from the ICA, where $\boldsymbol{B}_i = \boldsymbol{KJ}_i$ is the ith column of $\boldsymbol{B}$; the estimation of $\boldsymbol{J}_i$ denoted by $\overline{J_i}$ is given by the LORETA algorithm:

$$\overline{J_i} = (KW)^{+}\overline{B_i} \tag{5.5}$$

where $\boldsymbol{A}^{+}$ denotes the Moore–Penrose pseudoinverse of matrix. Thus, a low resolution tomography for a specific brain activity can be generated by this algorithm. This ICA-

LORETA method has been verified by numerical simulation and experimental tests using a volume conductor platform and fMRI, as shown in the following sections.

5.2 Verification by Numerical simulation results

A single layer sphere model (Wilson and Balyey 1950; Brody et al 1973), in which the brain is assumed to be a ball of homogenous volume conductor with unit radius, was used. The simulated EEG signal of two current dipoles located inside the ball along the x-axis with the coordinates (0, -0.5, 0) and (0, 0.5, 0), respectively, were generated by function generators, as shown in Fig. 5.1. The current amplitude of the two dipoles were varying with the time independently, which denoted by S1, S2 respectively. The waveforms of S1, S2 are shown in Fig.5.2. The simulated signals on the surface of the brain were mixture of the two sources, as shown in the Fig. 5.3. At a particular instant t, which is denoted in Fig. 5.3, the signal potentials on each channel were used to reconstruct the source tomography by LORETA. The 2-D tomography at the plane z=0 is shown in Fig. 5.4. The simulated singles were decomposed by ICA obtaining the two original sources and the coefficient maps of these sources, as shown in Fig. 5.5 and Fig. 5.6. The tomograph was reconstructed by LORETA using the coefficient maps. The 2-D tomography at the plane z=0 is showed in Fig 5.7. It is obvious that LORETA based on single-trial data can only give low-resolution tomography and can not separate the two current dipoles, as shown in Fig.4, while ICA based on LORETA, as shown in Fig 5.7(a) and Fig 5.7(b), can clearly indicate the different locations of the two dipoles.

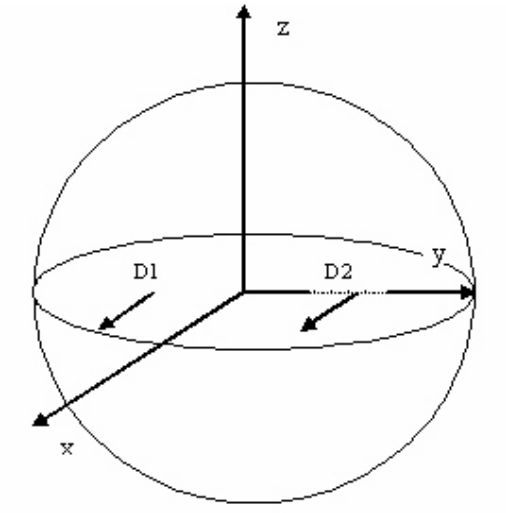

Figure 5.1 Single Sphere model with two current dipoles D1 and D2

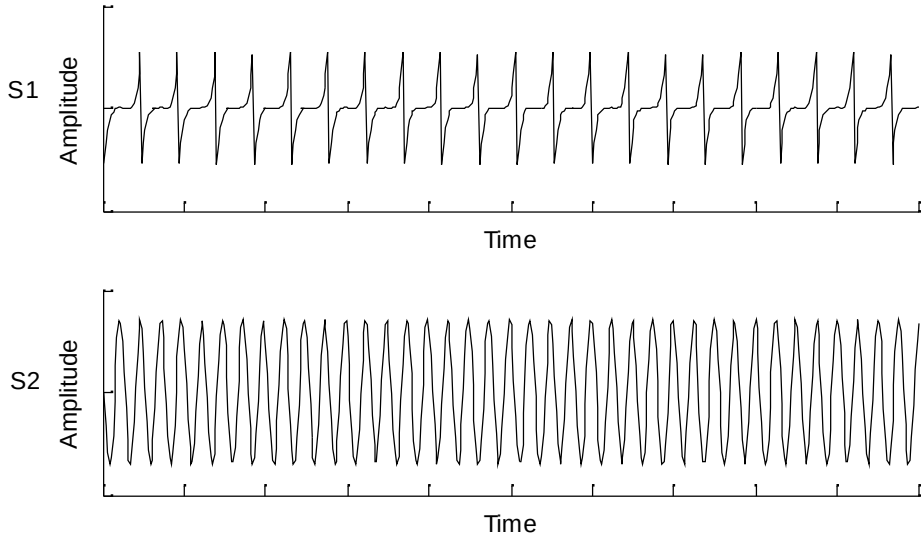

Figure 5.2 The waveforms of S1 and S2

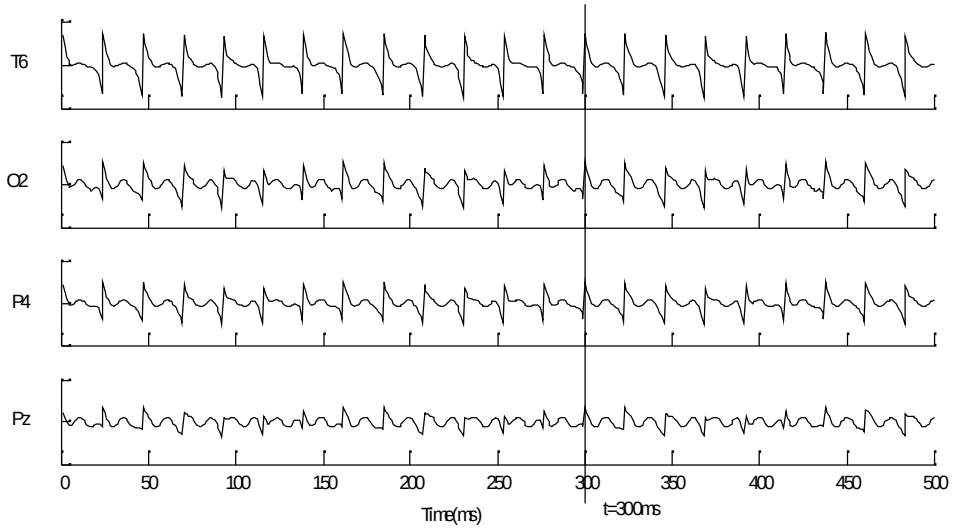

Figure 5.3 Four channels of the simulated EEG signals, the vertical line indicates the specific time instant at t=300ms

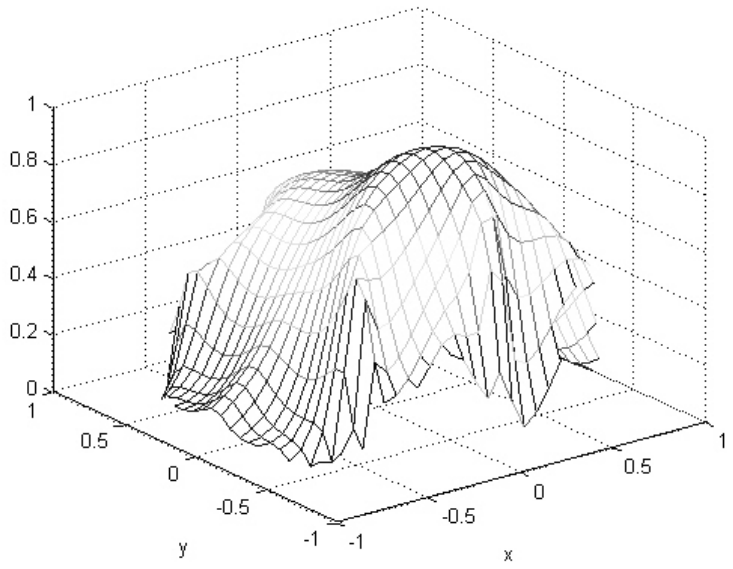

Figure 5.4 The tomography reconstructed by LORETA

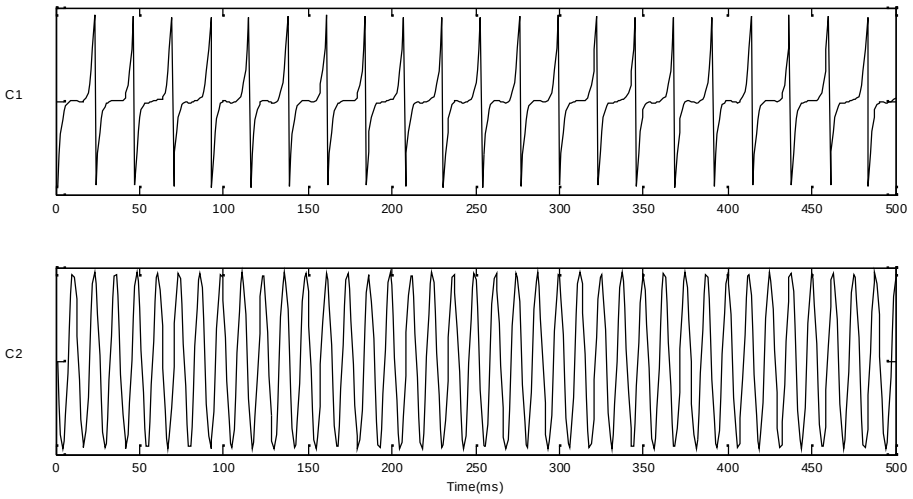

Figure 5.5 The two independent components separated by ICA. The first one was source S1 and the second one was source S2

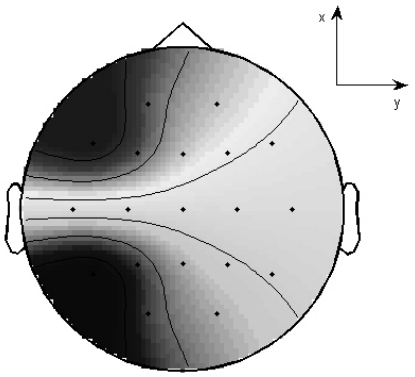

(a)

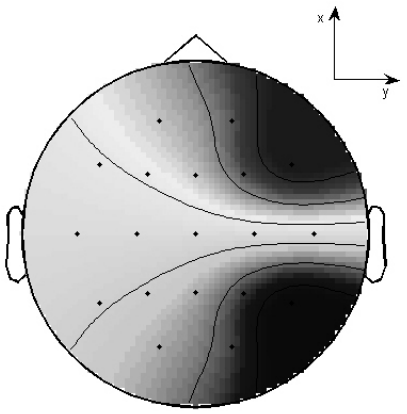

(b)

Figure 5.6 The coefficients map of the Independent components (a) the first independent component (b) the second independent component. The maps were gray scaled, dark represents large amplitude.

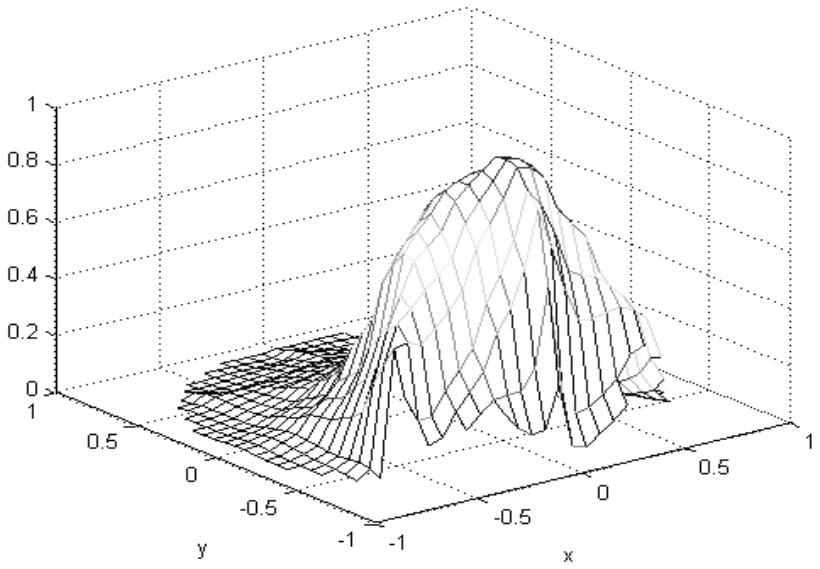

(a)

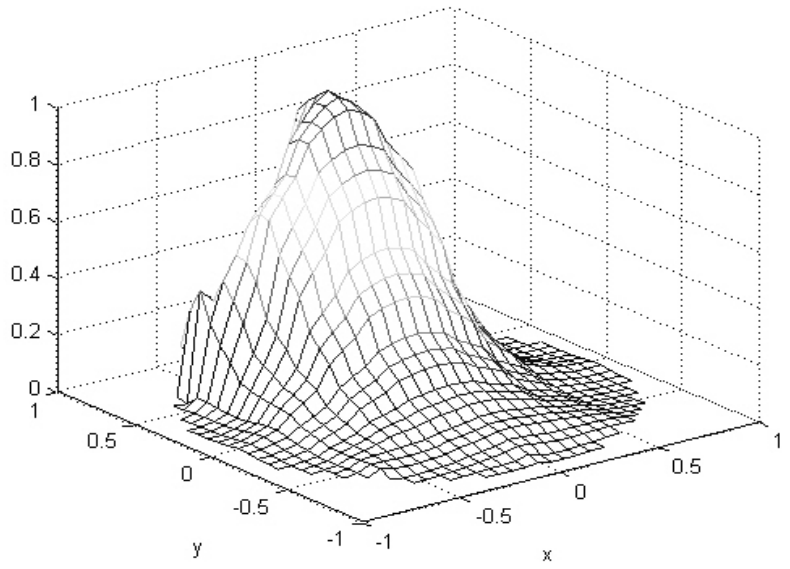

(b)

Figure 5.7 The tomography reconstructed by LORETA using the coefficient maps of (a) the first independent component (b) the second independent component

5.3 Experimental verification using a volume Conductor

To validate that ICA-LORETA can locate specific brain activity sources, a simulated experiment using a volume conductor platform was conducted. The test was designed based on the fact that watermelon has some physical characters similar to the human head. Firstly they are both spherical volume conductor. Secondly they are both composite with different layers of different electrical resistances. These make watermelon an ideal model of the human head in the test.

5.3.1 Experimental setup

In the test setup, signal generators were used to simulate the electric sources in the brain. The simulated signals were injected into the watermelon through the spinal electrodes. The output signals were tested on the surface of watermelon. 19 electrodes

according to the standard 10-20 system were used to measure the signals on the watermelon surface and PL-EEG Wavepoint system was used to record the measured signals, as shown in Fig.5.8.

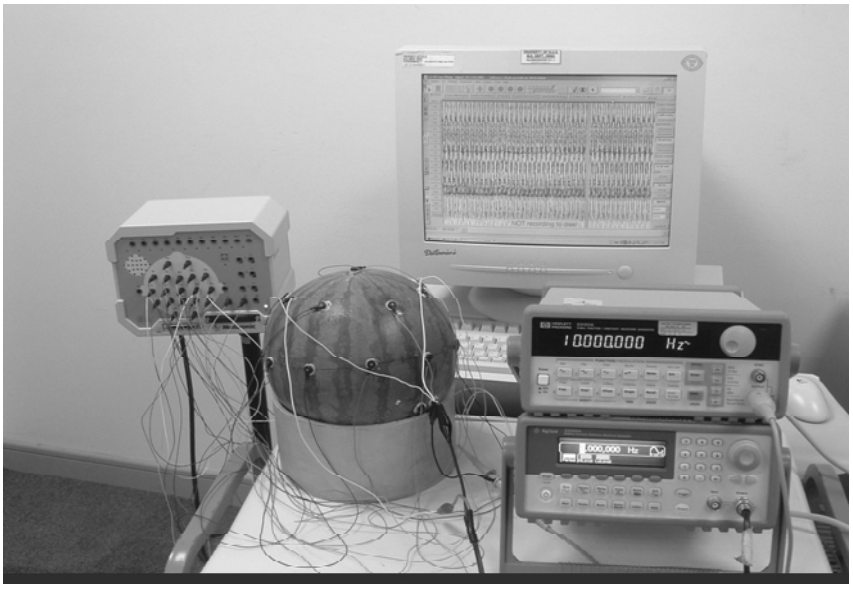

Figure 5.8 Devices of watermelon experiment

5.3.2 Results of the watermelon experiment

10 Hz and 5 Hz sine wave signals were used as the simulated sources. Fig. 5.9 shows the 4 channels of mixed signals measured on the surface on the watermelon. Fig. 5.10 shows the first four ICA components. It can be seen that the two sine wave sources are separated in C2 and C4, where C1 and C3 are noise. The coefficient maps of C2 and C4 are shown in Fig. 5.11. The location of the two sources are (0.3, 0.3, 0.8) and (0.3,-0.3, 0.8). The max value of the tomography of LORETA from the coefficient map of C2 is at (0.2793, 0.3414, 0.7759) and the max value of the tomography of LORETA from the coefficient map of C2 is at (0.2793, -0.3414, 0.7759).

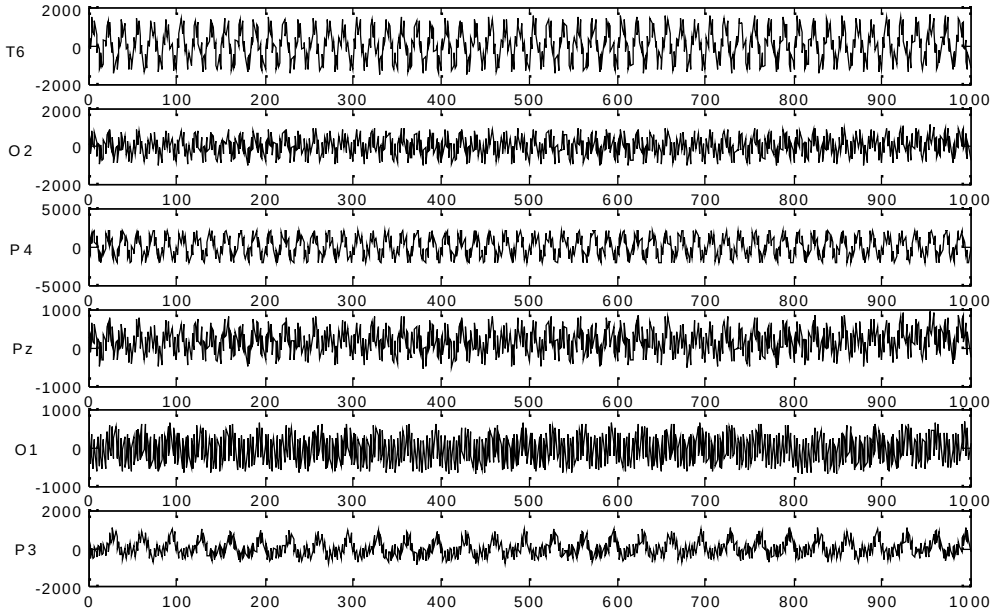

Figure 5.9 Six channels of measured mixed signals on the surface of watermelon, the sampling rate was100Hz

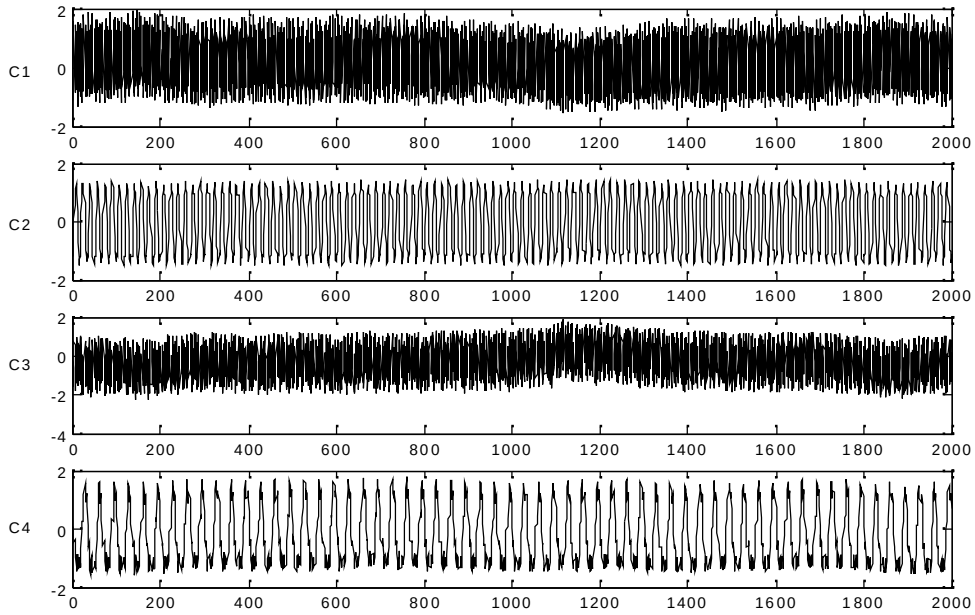

Figure 5.10 The first four independent components; the sampling rate was 100Hz

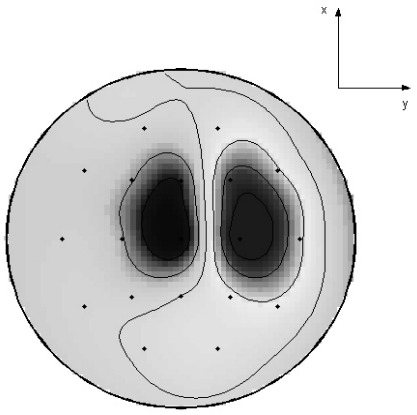

(a)

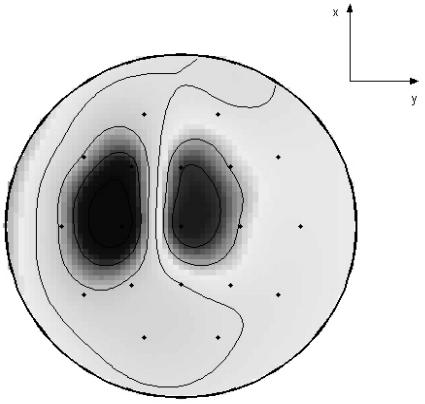

(b)

Figure 5.11 The coefficient maps of the independent components corresponding to sources. (a) C2 (b) C4. The maps were gray scaled, dark represents large amplitude.

The results show that the ICA-LORETA method can be used in the source separation and locating on the volume conductor, for example, the separation and locating of EEG signals on the human head.

5.4 Extraction of brain activities in response to irregular auditory stimulus

In previous research, ICA method was mainly used to separate artifacts from the EEG signals, using ICA method to identify certain brain activity was not widely reported yet. In our project, the attention shifting response to sudden hand clap and pop stimulus under quite environment was successfully identified in the ICA components and find the location of the sources in the brain. These responses can be observed directly in the montage channels Fz-Cz and Cz-Pz. In the ICA components separated from EEG raw data, it was found that only one component has an obvious peak at the same time when the response vertexes appear in the montage channels (Shen, K.Q, et al 2004). Moreover, the topographies reconstructed by the LORETA are similar indicating that these responses come from the same area of the brain.

Two sets of results are listed below. The first set includes experiment Pop1 and Pop2. From the time marking, the brain activity components corresponding can be identified to pop stimulus (Fig. 5.12, Fig 5.13, Fig 5.14 and Fig 5.15). Components of ECG signal are also clear. The coefficient maps are consistent in experiments Pop1 and Pop2. The similar results are presented in the second set which consists of experiment Clap1 and Clap2 for clap stimulus (Fig. 5.16, Fig 5.17, Fig 5.18 and Fig 5.19). The coefficients maps of the response related ICA components are consistent, as shown in the Fig. 5.20

Figure 5.12 Raw EEG montage data (experiment pop1).Two vertexes were observed in Fz-Cz and Cz-Pz channels due to the pop sound stimulus at 6th second.

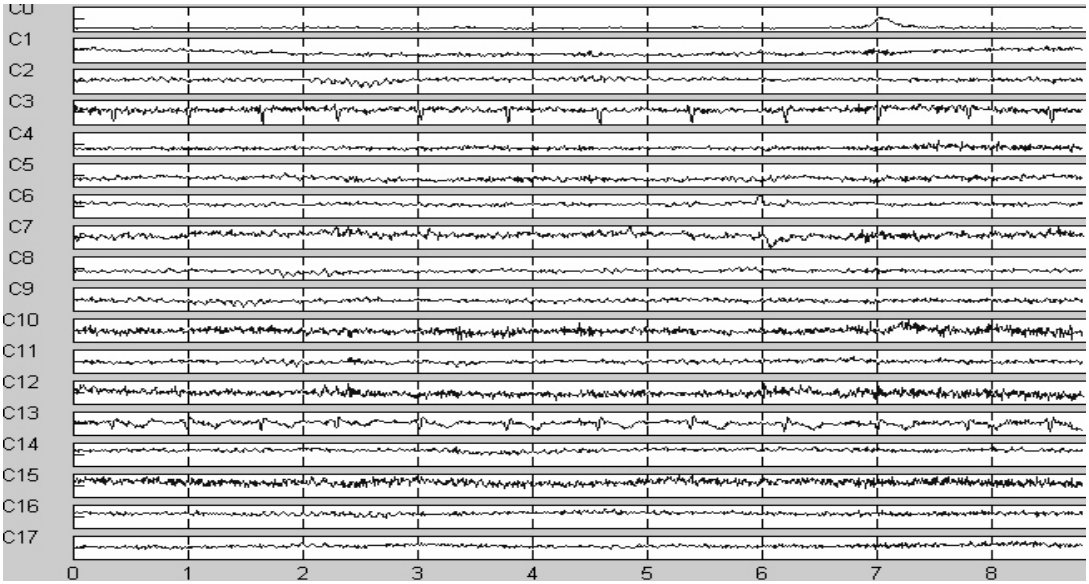

Figure 5.13 Component C6 was the brain response due to the pop sound stimulus according to Fig 5.12. C3 was the heartbeat artifacts (ECG)

Figure 5.14 Raw EEG montage data (experiment pop2). Two vertexes were observed in Fz-Cz and Cz-Pz channels due to the pop sound stimulus at about 7th second.

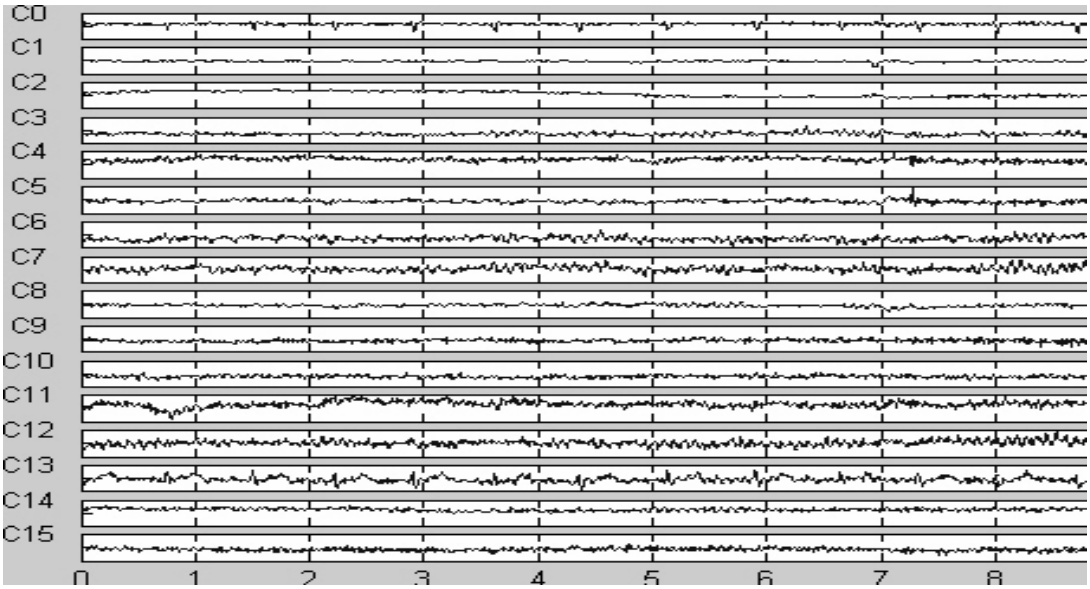

Figure 5.15 Component C1 was the brain response due to the pop sound stimulus according to Fig 5.14. C0 was the heartbeat artifacts (ECG)

Figure 5.16 Raw EEG montage data (experiment clap1). Two vertexes were observed in Fz-Cz and Cz-Pz channels due to the clap sound stimulus after 8h second.

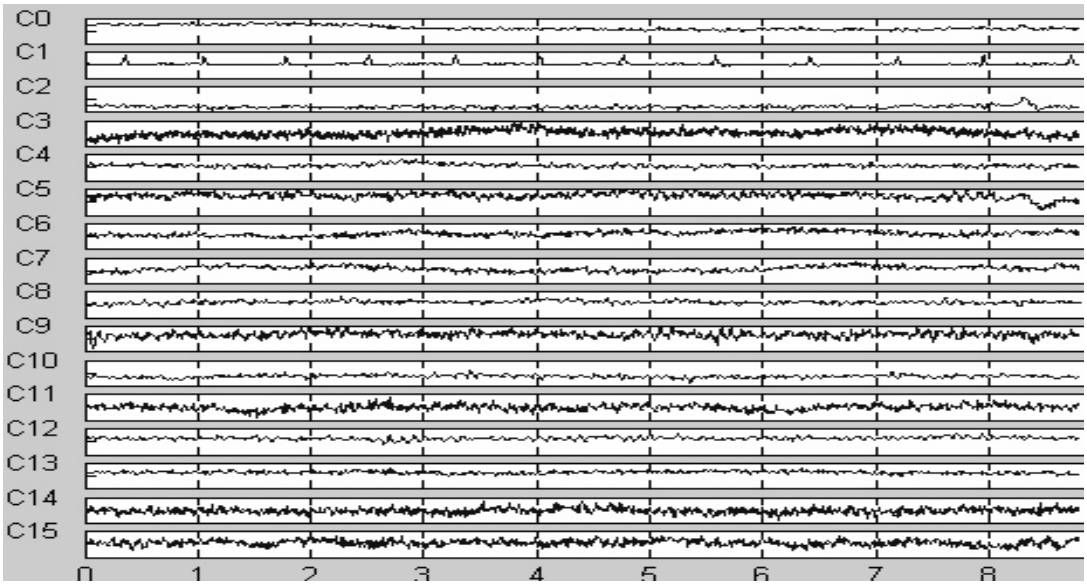

Figure 5.17 Component C2 was the brain response due to the clap sound stimulus according to Fig 5.16. C1 was the heartbeat artifacts (ECG)

Figure 5.18 Raw EEG montage data (experiment clap2). Two vertexes wre observed in Fz-Cz and Cz-Pz channels due to the clap sound stimulus

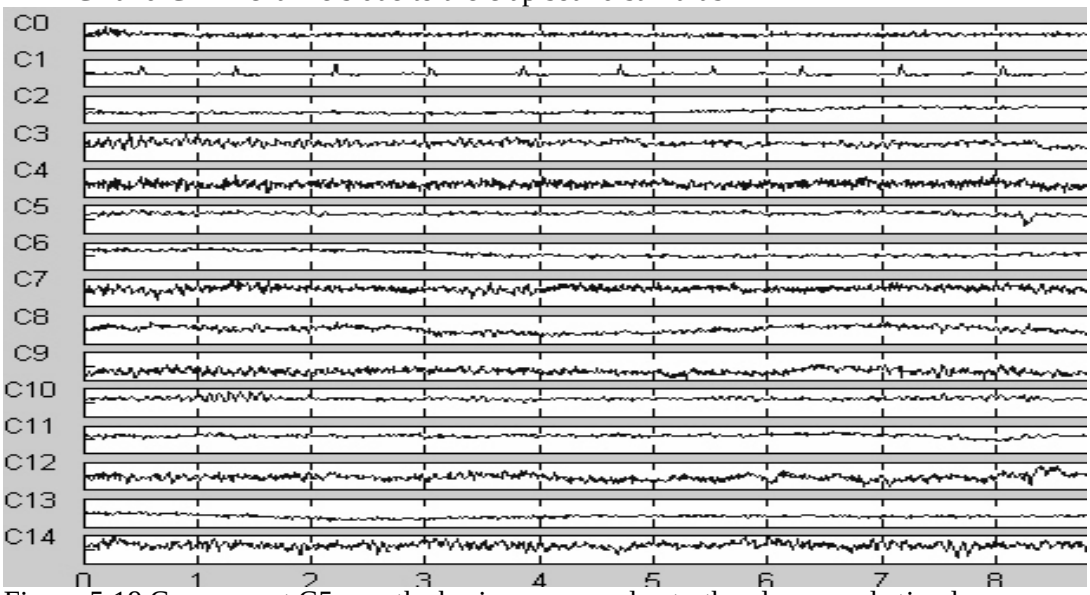

Figure 5.19 Component C5 was the brain response due to the clap sound stimulus according to Fig 5.18. C1 was the heartbeat artifacts (ECG**)**

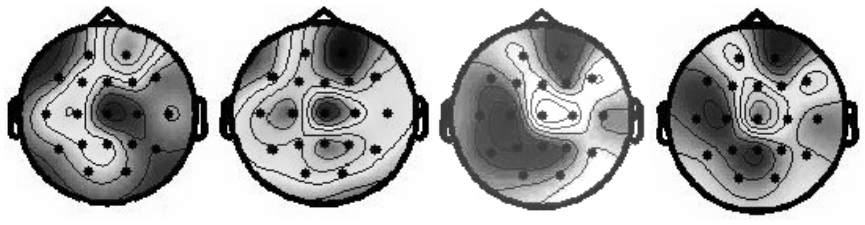

Figure 5.20 Coefficient maps of ICA components corresponding to response, the maps were gray scaled, dark represents large amplitude.

The tomography reconstructed by LORETA using the ICA coefficient maps are showed in Fig 5.21, Fig 5.22, Fig 5.23, Fig 5.24. The dark area (indicated by the arrow) shows the location of brain activity sources. From the tomography, it is shown that the sources of the responses are all concentrated in the medial frontal gyrus area indicating that the responses are caused by infrequent auditory stimulus (Christoph Mulert, et al 2004; David Friedman, ea al, 2001; Muller, B. W, ea al 2003). The results are also cross-validated by fMRI. For the auditory stimulus in fMRI, there are two kinds of stimulus, 1000Hz tone (infrequent target: 8%) or tone of other four frequencies,200Hz, 300Hz, 500Hz or 700Hz(frequent un-target 92%) bursts (500ms duration) were presented to the subject. Although, the stimulus of ICA-LORETA and fMRI were not exactly the same, and the subjects are not the same, the brain activities measured were the same, therefore the source location should be the same.

The fMRI scanned during the infrequent target stimulus shows that there is a common active area between fMRI and LORETA, see Fig. 5.25. In the fMRI, there were other active areas which corresponding to other kind brain activities, but they are not covered by ICA-LORETA, as ICA-LORETA has filtered out other brain activities and remained the specific one.

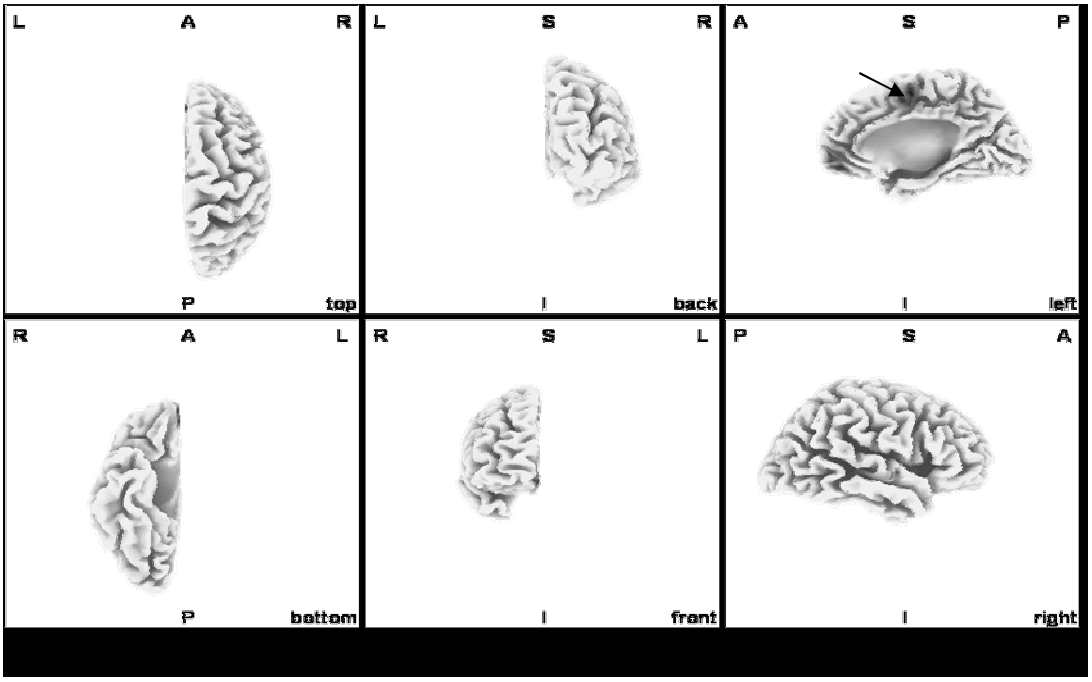

Figure 5.21 Tomography of ICA component C6 in experiment (Pop1) reconstructed by LORETA

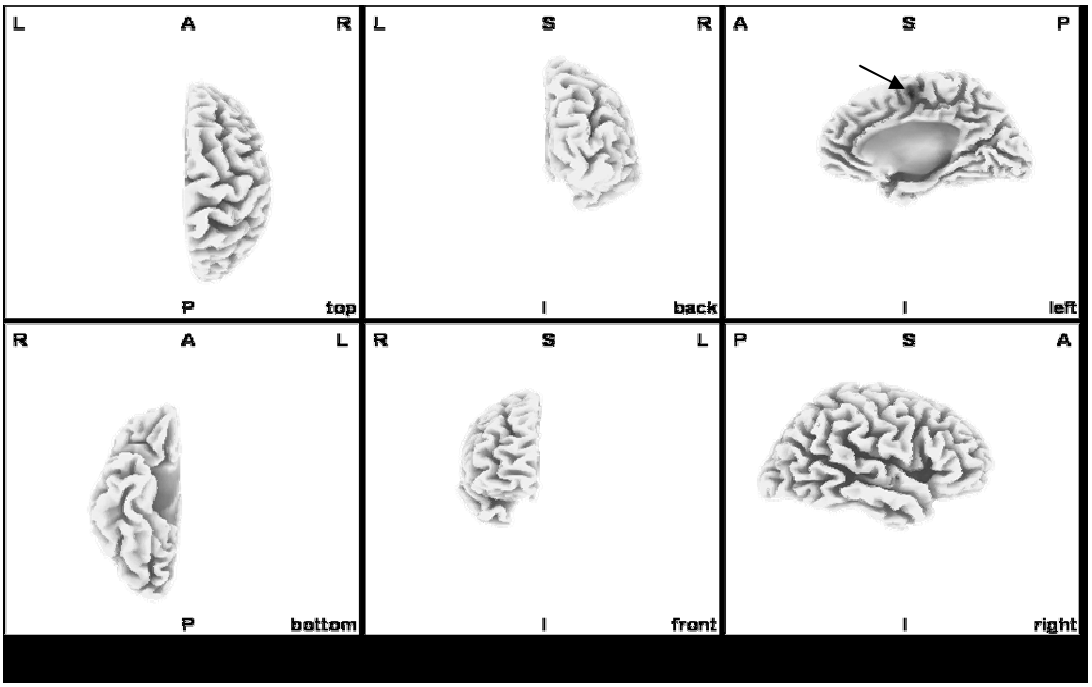

Figure 5.22 Tomography of ICA component C1 reconstructed by LORETA, in experiment (Pop2)

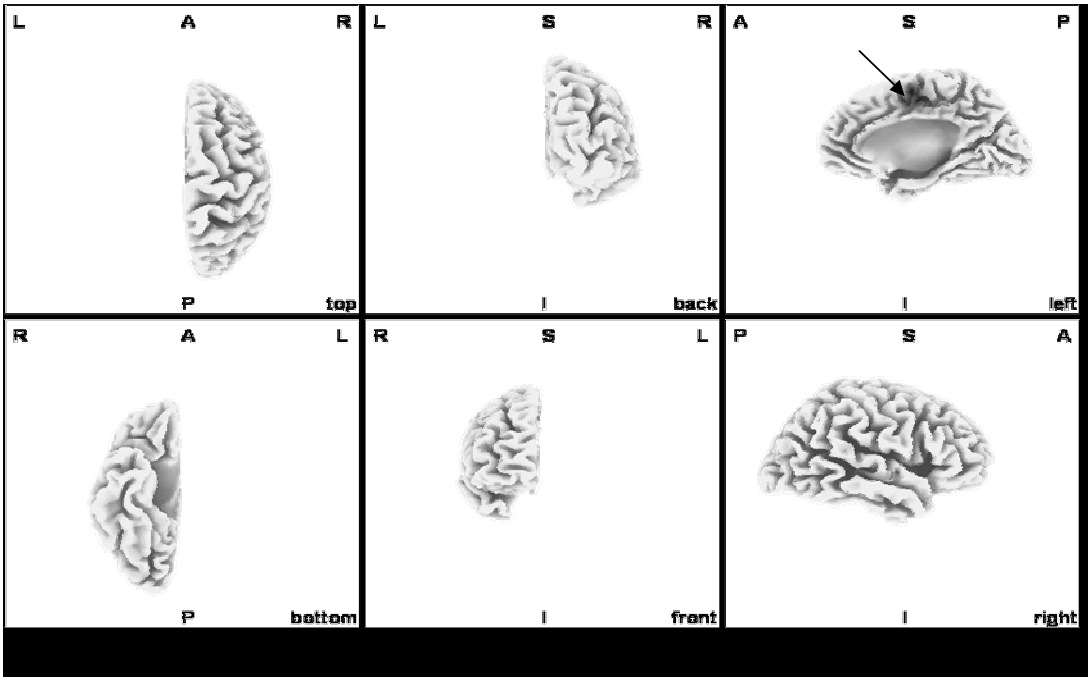

Figure 5.23 Tomography of ICA component C2 reconstructed by LORETA, in experiment (Clap1)

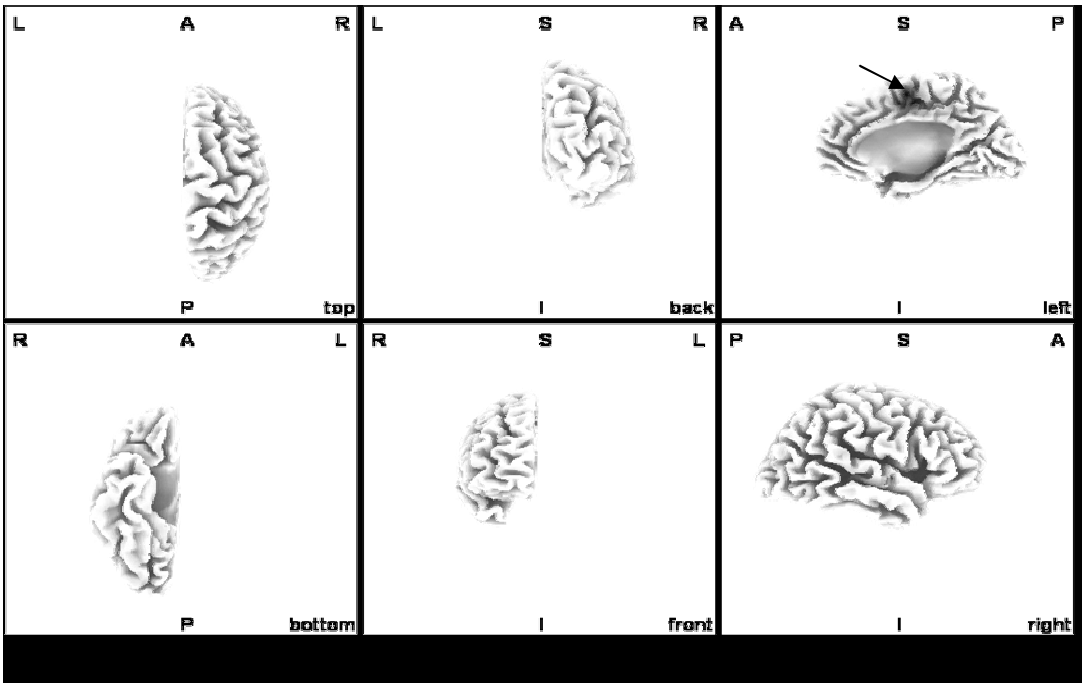

Figure 5.24 Tomography of ICA component C5 reconstructed by LORETA, in experiment (Clap2)

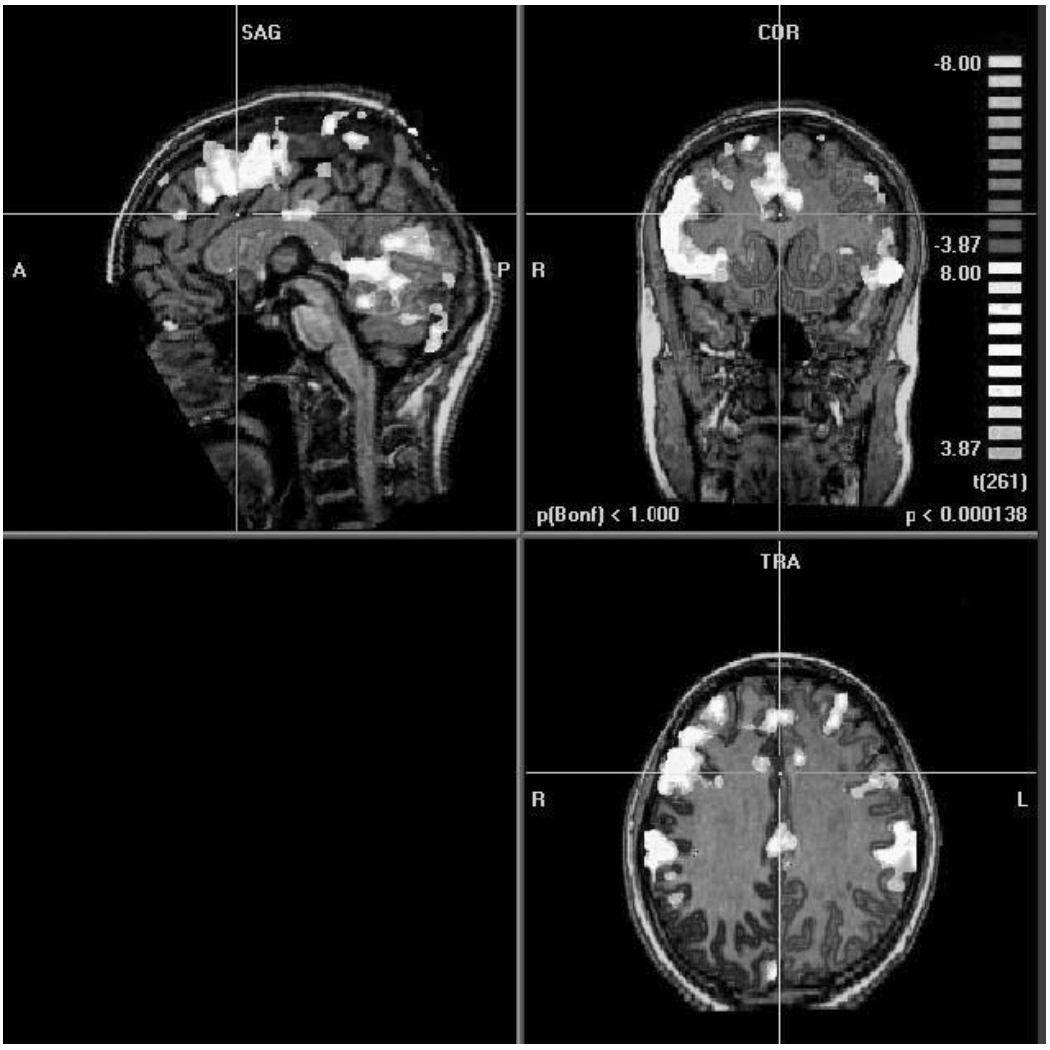

Figure 5.25 Pictures showing activation regions corresponding to infrequent target stimulus, where the light areas were in activation.

Chapter 6

CONCLUSIONS

ICA is a powerful algorithm for blind signal processing and is very suitable for EEG signal decomposition. Combined with other algorithms, ICA can be used in automatic artifact removal, locating specific brain activity in the brain with promising results.

(1) A novel volume conductor brain activity simulation platform for validation of EEG signal processing methods has been presented. The platform consists of a volume conductor, spinal electrodes inserted into the volume conductor and function generators. By controlling the amplitude and waveform of signals generated by the function generators, a volume conductor brain activity simulation platform can be established, on which electric potentials at different locations can be measured. The measured signal together with the information of dipole sources can be used for validation of EEG signal processing methods. The simulation platform has been used in the validation of ICA in EEG signal decomposition and the validation of the spatial power mapping method for EEG analysis.

(2) The experiment on the proposed volume conductor platform showed that ICA can successfully decompose mixed source signals on the human head and is robust to hardware and environmental noise. ICA can separate bioelectrical artifacts and hardware noise from raw EEG data as well as different brain activities. This conclusion is very important, since ICA is widely used in EEG artifact removal and is combined with LORETA in this research to locate specific brain activity using single-trial EEG data. However, the conclusion was not strongly supported by the validation of actual experiment on the human head or a similar volume

conductor platform in the previous study. All previous validation of ICA for EEG signal decomposition is numeric simulation without considering whether the liner mixture model is available on the real human head under the real noisy environment. The experiment on the novel platform provides a strong validation of this basic assumption for the application of ICA in EEG signal decomposition.

(3) It has been verified by both experiment on the proposed platform and the previous research, ICA can separate artifacts from EEG signals with good accuracy. But the artifacts of EEG are quite different from each other both in time and frequency domain, using one model to identify all artifact components is not possible. Thus algorithms to identify artifactal independent components were developed for ECG artifact and EOG artifact in this research respectively. The algorithms require little computation but proved to be efficient. The experiments on real raw EEG data proved that these algorithms can automatically remove EOG and ECG artifacts without overcorrection and can be used in online EEG data processing.

(4) It is needed to point out that for EOG artifact removal, 4 additional channels of EOG are used to identify the EOG independent components. This is also required for many other EOG artifact correction methods and acceptable in most cases. Since most of EEG machines have additional channels for EOG recording, and the increased data is small compared with 19 or even more channels of EEG data, it will not bring any problem in the data recording and processing. The electrodes around the eye will not bring any baleful affect to the subject during the test.

(5) The ICA-LORETA exploits the temporal characteristics of the signal in addition to the spatial conditions to solve the EEG inverse problem. The results of numerical simulation and an real experiment on a volume conductor show that by introducing ICA to separate signals, the shortcoming of LORETA that it can not separate sources nearby has been overcome without invalidating the "smoothest"condition of LORETA while other improvements of LORETA (Zhou, J. et al 2004) do not remain this condition. If the sources of brain activities are smoothly distributed and independent of each other, this algorithm can give better result than the LORETA and algorithms based on dipole model. If the sources are diploes or highly concentrated, it's worse than the algorithms based on dipole model and the improvements of LORETA based on the "highly concentrated" condition, but it is still better than the original LORETA when the independent condition is available.

(6) Then fMRI shows that the active area in the human brain reacting to the external stimulus is not highly concentrated as dipoles but more likely to be smoothly distributed in the area with specific neural function. This proves that the distributed model used in LORETA is more reliable than the dipole model and the "smoothest" condition should be hold.

(7) The tomography of ICA-LORETA and fMRI has the common active area, showing that the ICA-LORETA can locate event-related stimulated brain activity from single-trial EEG data with good accuracy. This is a promising result, since the original LORETA can only process averaged ERP signal.

(8) The ICA-LORETA can also be applied to spontaneous EEG measurement besides the single-trial Even Related Potential. This is an attractive virtue which neither original LORETA nor fMRI possesses, since most of the brain activities not even related but spontaneous.

Chapter 7

FUTURE WORK

(1) A new algorithm for automatic identification of OA components which does not need additional EOG channels will be developed in future. The new algorithm will utilize time _frequency features and the propagation pattern of ocular artifacts on the scalp instead of regression on the EOG channels.

(2) The ICA-LORETA algorithm will be applied in more brain activities especially in the spontaneous brain activities in future. Since most of the studies were concentrated at the event related brain activities and few work were done on spontaneous brain activities because of difficult in separating and locating such activities, the ICA-LORETA algorithm can help us to understand more about the spontaneous brain activities

References

Barlow, J. S. and Dubinsky, J., "EKG-artifact minimization in referential EEG recordings by computer subtraction," *Electroencepb.clin. Neurophysiol*., vol.48, pp.470-472, 1980

Brody, D. A., Terry, F. H. and Ideker, R. E., " Eccentric dipole in a spherical medium: generalized expression for surface potentials," *IEEE Trans. Biomed. Eng.*, vol.20 pp.141–143, 1973

Bland, B. H. and Colom, L.V., "Extrinsic and intrinsic properties underlying oscillation and synchrony in limbic cortex," *Progr. Neurobiol*, vol.41, pp.157-208, 1993

Coifman, R. R. and Donoho, D. L., "Translation invariant de-nosing," *Lecture Notes in Statistics*, vol.103, pp.125-150, 1995

Comon, P. "Independent component analysis—A new concept?" *Signal Processing*, vol.36, pp.287–314, 1994

Croft, R.G. and Barry, R. G. "Removal of ocular artifact from the EEG: a review" *Neurophysiology, Clinic*, vol.30, no.1, pp.5-19, 2000

Croft, R.G. and Barry, R. G., "EOG correction: a new aligned-artifact average solution" *Electroenceph. Clin. Neurophysio*. vol.107, no.6, pp. 395-401, 1998

Cuffin, B. N. and Cohen, D., "Comparison of the magnetoencephalogram and electroencephalogram," *Electroencephalogr. Clin. Neurophysiol.*, vol.47: 132–146, 1979

Cuffin, B. N., Cohen D, Yunkuchi, K., Maniewski, R., Purcell, C., Cosgrove G. R., Ives, J., Kennedy, J. and Schomer, D., "Test of EEG localization accuracy using implanted sources in the brain," *Ann Neurol.* vol.29 no.2, pp.132-138, 1991

Cuffin, B. B., "A method for localizing EEG sources in realistic head models" *IEEE Trans. Biomed. Eng.*, vol. 42, pp.68–71, 1995

David Friedman, Yael M. Cycowicz, Helen Gaeta, "The novelty P3: an event-related brain potential (ERP) sign of the brain's evaluation of novelty," *Neuroscience and Biobehavioral Reviews*, vol.25, pp.355-373, 2001

Du, W. Z., Leong, H. M. and Gevins, A. S., "Ocular Artifact Minimization by Adaptive Filtering." *Statistical Signal and Array Processing*, IEEE Seventh SP Workshop, pp.433 - 436, 1994

Engel, A. K., Konig, P., Gray, C.M. and Singer, W., "Stimulus-dependent neuronal oscillations in cat visual cortex: intercolumnar interaction as determined by cross-correlation analysis." *Eur. J. Neurosci.*, vol.2, pp. 588-608, 1990

Hyvarinen, A., "Fast and robust fixed-point algorithms for independent component analysis," *IEEE Trans. Neural Networks*, vol.10, no.3, pp.626-634, 1999

Hyvarinen, A. and Oja, E, "Independent component analysis: algorithms and applications," *Neural Networks*, vol.13 (4-5), pp. 411-430, 2000

Ishiyama, Y., Ebe, M., Homma, L. and Abe, Z., "Elimination of EKG artifacts from EEGs recorded with balanced non-cephalic reference electrode method," *Electroenceph. clin. Neurophysiol.*, vol.53, no.6, pp.662-665, 1982

Jutten, C. and Herault, J. "Blind separation of sources, part I: An adaptive algorithm based on neuromimetic architecture," *Signal Processing*, vol. 24, pp.1–10, 1991

Gray, C. M., Engel, A.K. and Singer, W. "Oscillatory responses in cat visual cortex exhibit inter-columnar synchronization which reflects global stimulus patterns." *Nature*, vol.338, pp.334-337, 1989

Karhunen, J., Oja, E., Wang, L., Vigario, R. and Joutsensalo, J. "A class of neural networks for independent component analysis," *IEEE Trans. Neural Networks*, vol.8, pp.486–504, 1997

Kenemans, J. L., Molenaar, P. C., Verbaten, M. N. and Slangen, J. L., "Removal of the eye-movement artifact from the EEG: a comparison of time and frequency domain methods with simulated and real data," *Psychophysical*, vol.28, no.1, pp.114-121, 1991

Larsen, L. H., Prinz, P. N. and Moe, K. E., "EEG diagnosis of Alzheimer's disease methodology.", In preparation,1991

Llinas, R. R. "The intrinsic electrophysiological properties of mammalian neurons: insights into central nervous system function," *Science*, vol.242, pp.654-1664, 1988

Liu, H. S., Yang, F. S., Gao, X. R. and Gao, S. K., "Shrinking LORETA-FOCUSS: A Recursive Approach to Estimating HighSpatial Resolution Electrical Activity in the Brain" *Proceedings of the 1st International IEEE EMBS conference on Neural Engineering*, 2003

Mosher, J.C. and Leahy, R.M., "Recursive MUSIC: A framework for EEG and MEG source Localization," *IEEE Trans.*, vol.45, pp.342-1354, 1998

Muller, B., Stude, P., Neble, K. Wiese, H., Ladd, M. E., Forsting, M., Jueptner, M., "Sparse imaging of the auditory oddball task with functional MRI," *Neuroreport*, pp.14, no.12, pp.1597-1601, August 26, 2003

Musha, T., Okamoto, Y., "Forward and inverse problems of EEG dipole localization," *Critical Reviews in Biomedical Eng.*, vol.27, no.3-5, pp.189-239, 1999

Nakamura, M. and Shibasaki, H. "Elimination of EKG artifacts from EEG records: a new method of non-cephalic referential EEG recording," *Electroenceph. clin. Neurophysiol.*, vol.66, pp. 89-92, 1987

Nason, G. P. and Silverman, B. W., "The stationary wavelet transform and some statistical application", *Lecture Notes in Statistics*, vol. 103, pp. 281-289, 1995

Noda, A., "A modified FFT-based filter for noise reduction of EEG measurement in identifying learning processes," *Circuits and System, IEEE international Symposium, on 8-11 may*, vol.2, pp.1007, 1989

Okamoto, Y., Teramachi, Y., Musha, T., "Limitation of the Inverse Problem in Body Surface Potential Mapping," *IEEE Trans. BME* vol.30, pp.749-754, 1983

Pascual-Marqui, R. D., Michel, C. M. and Lehmann, D., "Low resolution electromagnetic tomography: a new method for localizing electrical activity in the brain", *International Journal of Psychophysiology*, vol.18, pp.49-65, 1994

Pascual-Marqui, R. D., "Review of methods for solving the EEG inverse problem" Int. J. *Bioelectrontagnetism*, vol.1, no.1, pp. 75-86, 1999

Rush, S. and Driscoll, D. A., "Current distribution in the brain from surface electrodes," *Anesth. Analg*., vol.47, pp.717–723, 1968

Rush, S., "On the independence of magnetic and electric body surface recordings," *IEEE Trans., BME* vol.22, pp.157-167, 1975

Scherg, M. and Picton, T. W., "Separation and identification of event-related potential components by brain electric source analysis, Event-Related Brain Research," *EEG Suppl.42* pp. 24-37, 1991

Shen, K.Q., Li, X. P., Cao, C., Yeo, M. and Smith, E.W., "Extraction of brain activity signal from EEG signals" *Journal of Clinic Neuroscience*, vol.11 sup.1, pp.70, 2004

Silva, L. R., Amitai, Y. and Connors, B. W., "Intrinsic oscillations of neocortex generated by layer 5 pyramidal neurons." *Science*, vol.251, pp.432-435, 1991

Sun, M. "An Efficient Algorithm for Computing Multishell Spherical Volume Conductor Models in EEG Dipole Source Localization" *IEEE Trans. Biomed. Eng*, vol.44, pp.12, 1997

Takano, N., Maruyama, T., Tarnagawa, M. and Yana, K., "EOG artifact canceling for EEG analysis using rls adaptive filtering technique**"**, *Proceedings of the 15th Annual International Conference of the IEEE* pp.348 - 349, Oct 28-31, 1993

Vigario, R. N., "Extraction of ocular artifacts from EEG using independent component analysis," *Electroencephalogr. Clin. Neurophysiol*, vol.103, no.3, pp.395-404, 1997

Venkata, S., "A Novel Wavelet Based Technique for Detection and De-noising of Ocular Artifacts in Normal and Epileptic Electroencephalogram," *Proceedings of IEEE International Conference on Signal Processing (ICSP)*, 2004

Wang, J.,Williamson, S. J. and Kaufman, L., "Magnetic source images determined by a lead-field analysis: the unique minimum-norm least-square estimation," *IEEE Trans., BME* vol.39, pp.665-675, 1992

Wei, D. and Gotman, J. "Removal of ECG artifact from EEG Using ICA," *Proceedings of the second joint EMBS/BMES Conference*, pp.206-207, 2002

Wilson, F. N. and Bayley, R. H., "The electric field of an eccentric dipole in a homogeneous spherical conducting medium," *Circulation vol*.1 pp.84–92, 1950.

Woestenburg, J. C., Verbaten, M. N. and Slangen, J. L., "The Removal of the eye-movement artifact from the EEG by regression analysis in the frequency domain," *Biological Psychology* vol.16, pp.127- 147, 1983

Zou, J., Xie, Y. Q., Yuan, J. S., Ma, X. S., Cui, X., "Source region contracting method for EEG source reconstructions," *IEEE Trans. Magnetics*, vol.40, no.2, pp.1128 – 1131, 2004

LIST OF PUBLISHED WORK IN THE THESIS

C. Cao, X.P. Li, H. Zheng, K.Q. Shen, Y.Y. Pang, E.P.V. Wilder-Smith, "A novel simulation platform for validation of EEG signal processing methods", 57th Annual Meeting of the American Academy of Neurology (AAN), Miami, United States, 2005

K.Q. Shen, X.P. Li, C. Cao, M.V.M. Yeo, E.P.V. Wilder-Smith, "Extraction of brain activity signals from EEG signals", 11th Asian & Oceanic Congress of Neurology (AOCN), Singapore; Journal of Clinical Neuroscience, Vol. 11, Sup. 1, November, 2004

C. Cao, X.P. Li, Y.Y. Pang, K.Q. Shen, H. Zheng, "Automatic EOG artifact removal based on independent component analysis and stationary wavelet transform de-noising", 11th Asian & Oceanic Congress of Neurology (AOCN), Singapore; Journal of Clinical Neuroscience, Vol. 11, Sup. 1, November, 2004

Y.Y. Pang, X.P. Li, W. Zhou, C. Cao, K.Q. Shen, E.P.V. Wilder-Smith, "Development of a new method for screening of mental fatigue", 11th Asian & Oceanic Congress of Neurology (AOCN), Singapore; Journal of Clinical Neuroscience, Vol. 11, Sup. 1, November, 2004

C. Cao, X.P. Li, E.P.V. Wilder-Smith, "A novel simulation platform for validation of EEG signal processing methods", Neurology (submitted for publication)

C. Cao , X.P. Li, E.P.V. Wilder-Smith, “ICA based LORETA for brain activity source locating” International Journal of Psychophysiology (submitted for publication)